RICE UNIVERSITY

Screened Coulomb Hybrid Density Functionals

by

Jochen Heyd

A Thesis Submitted
in Partial Fulfillment of the
Requirements for the Degree

Doctor of Philosophy

Approved, Thesis Committee:

Gustavo E. Scuseria, Chairman
Robert A. Welch Professor of Chemistry

Bruce Johnson
Senior Faculty Fellow, Chemistry Department

Peter J. Nordlander
Professor of Physics

Houston, Texas

April, 2004

Abstract

Screened Coulomb Hybrid Density Functionals

by

Jochen Heyd

The screened Coulomb hybrid density functional theory developed in this work extends the applicability of hybrid functionals to large molecules and solids. Traditional hybrid functionals have been applied to medium sized molecules and some insulating solids with excellent results. However, the fundamentally long range of the Hartree-Fock (HF) exchange interaction limits their use for biomolecules and semi-conducting or metallic solids.

The large spatial extent of the HF exchange can be reduced by utilizing a screened Coulomb potential. Such potentials have been widely used in solid state physics. Efforts of employing them in quantum chemistry were not as successful due to the unsatisfactory accuracy of the resulting methods. This work takes a new approach by combining a screened HF potential with both short and long range screened density functionals. The Heyd-Scuseria-Ernzerhof (HSE) screened Coulomb hybrid density functional is designed to produce exchange energies comparable to traditional hybrids while only using the short range, screened HF exchange.

The accuracy of the HSE functional is assessed on a wide range of molecules and solids. Enthalpies of formation, geometries and vibrational frequencies of the G3 set of 223 molecules are predicted with performance equivalent to the best traditional hybrids. A set of 21 insulating, semi-conducting and metallic solids was used to determine the accuracy of lattice constants and bulk moduli. Both properties show significantly improved accuracy, compared to pure density functionals. HSE also accurately predicts band gaps of semi-conductors whereas pure density functionals severely underestimate the band gaps.

Benchmarking of HSE in several semi-conducting and metallic solids shows a drastic decrease in computational cost, compared to established hybrid functionals. HSE achieves linear scaling for medium size systems (greater than 15 Å) whereas regular hybrids scale as $\mathcal{O}(N^{2.5})$ for systems up to 100 Å and scale linearly only beyond that. This late cross-over makes it computationally prohibitive to treat complex solids with traditional hybrid functionals. HSE circumvents this bottleneck and produces superior results while increasing computational cost by a factor of only two to four, compared to pure density functional theory.

Acknowledgments

I would like to thank Dr. Gustavo Scuseria for his guidance in accomplishing my research goals. Dr. Philippe Ayala, Dr. Juanita Jaramillo, Dr. Matthias Ernzerhof, Dr. Juan Peralta, Dr. Konstantin Kudin, and Sergey Maximoff were always available for very helpful discussions. I am also thankful to Dr. Viktor Staroverov, Dr. Verónica Barone, Dr. Hiromi Nakai, and Dr. Pere Constans for their input and collaboration in applying the HSE functional to a diverse array of systems.

During the course of my research, I have received financial support from Rice University, the Welch Foundation, the National Science Foundation (Grant No. CHE-9982156), and the Department of Energy SciDAC Computational Chemistry Program (Grant No. DE-FG02-01ER15232).

I would also like to especially thank Renee Baker, Hans and Heide Heyd for their continuous support and encouragement.

Contents

Tables

Figures

Preface

This thesis is based on parts of my research conducted at Rice University. Most of the results shown have been previously published in a series of papers:

- Jochen Heyd, Gustavo E. Scuseria, and Matthias Ernzerhof

  Hybrid functionals based on a screened coulomb potential

  J. Chem. Phys. **118**, 8207 (2003)

- Jochen Heyd and Gustavo E. Scuseria

  Assessment and validation of a screened Coulomb hybrid density functional

  J. Chem. Phys. **120**, 7274 (2004)

- Jochen Heyd and Gustavo E. Scuseria

  Efficient hybrid density functional calculations in solids:

  Assessment of the HSE screened Coulomb hybrid functional

  J. Chem. Phys., accepted (2004)

In addition, the HSE functional has been applied to several other solids. Collaborating with Verónica Barone, I studied interactions of single-walled carbon nanotubes with both hydrogen and oxygen:

- Verónica Barone, Jochen Heyd, and Gustavo E. Scuseria

  Interaction of atomic hydrogen with single-walled carbon nanotubes: A density

functional theory study

J. Chem. Phys. **120**, 7169 (2004)

- Verónica Barone, Jochen Heyd, and Gustavo E. Scuseria

  Effect of oxygen chemisorption on the energy band gap of a chiral semiconducting single walled carbon nanotube

  Chem. Phys. Lett., accepted (2004)

Other research, yet to be published, included both the rutile and anatase phases of TiO_2 (with Hiromi Nakai) and combining screened Hartree-Fock exchange with screened correlation density functionals (with Pere Constans).

Chapter 1

Introduction

Kohn–Sham density functional theory (DFT) has proven to be a highly competitive method for a wide range of applications in solid state physics and more recently in chemistry. While the local density approximation (LDA) [1] has been used in solid state physics for quite some time, the advent of functionals based on the generalized gradient approximation (GGA) [2] has made DFT a valuable tool in chemistry. Hybrid density functionals [3], which include a certain amount of Hartree-Fock (HF) exchange, have further improved upon the GGA results. For molecules, recently developed meta–GGA functionals [4] have been shown to yield accuracy comparable to hybrid functionals [5]. In addition, meta–GGAs yield significant improvements in solids [6]. However, a comparison with hybrid functionals in solids is difficult due to the high computational demands of traditional hybrids.

The ground-state Kohn–Sham [1] energy of a system is given by

$$E = E_{Ne}(\rho) + T_s(\rho) + J(\rho) + E_{\mathrm{xc}}(\rho) \tag{1.1}$$

where ρ is the total electron density, E_{Ne} is the nuclear–electron attraction, T_s is the non–interacting kinetic energy, J is the Coulomb repulsion of the electrons and E_{xc} is the exchange–correlation energy. All components of Eq. 1.1 are known exactly

with the notable exception of the exchange–correlation energy. Many properties of the exact E_{xc} are known, but the specific form of this term is unknown. Better approximations for E_{xc} are one of the main research foci in DFT, as well as in this work.

Methods scaling linearly with system size [7] are available for pure DFT calculation, allowing simulations of large molecules and solids. However, the HF exchange in hybrid DFT methods is much less tractable in large systems. Schemes for linear scaling HF calculations depend on the natural decay of the HF exchange interactions over distance. This decay is highly system dependent and can range from a few Ångstrøm to thousands of Ångstrøm [8, 9]. A general hybrid DFT method which can be used over a wide range of system sizes is highly desirable. Screened Coulomb hybrid functionals, presented here, are a possible approach to such a method.

To render the HF exchange tractable in extended systems, either the exchange interactions need to be truncated artificially or their spatial decay accelerated. Truncation schemes are very useful for systems with localized charge distributions where the HF exchange decays rapidly over distance. In delocalized systems, however, truncation leads to severe convergence problems in the self-consistent field (SCF) procedure as well as uncertainties in the predicted energy of the system. The second option, accelerating the spatial decay, circumvents both these problems but still neglects interactions which might be physically important. The present work takes this second approach but attempts to compensate for the neglected interactions.

The decay of the HF exchange interaction can be accelerated by substituting the full $1/r$ Coulomb potential with a screened potential. Such screened Coulomb potentials are widely used in solid state physics [10] and more recently also in quantum chemistry [11, 12, 13, 14, 15]. A screened Coulomb potential is based on a split of the Coulomb operator into short range (SR) and long range (LR) components. The choice of splitting function is arbitrary as long as SR and LR components add up to the original Coulomb operator. The present work uses the error function to accomplish this split since it leads to computational advantages in evaluating the short range HF exchange integrals (see Section 2.1). The following partitioning is used:

$$\frac{1}{r} = \underbrace{\frac{\mathrm{erfc}(\omega r)}{r}}_{\mathrm{SR}} + \underbrace{\frac{\mathrm{erf}(\omega r)}{r}}_{\mathrm{LR}} \tag{1.2}$$

where the complementary error function $\mathrm{erfc}(\omega r) = 1 - \mathrm{erf}(\omega r)$ and ω is an adjustable parameter. For $\omega = 0$, the long range term becomes zero and the short range term is equivalent to the full Coulomb operator. The opposite is the case for $\omega \rightarrow \infty$.

The decay properties of the full exchange interaction and its screened counterpart can be illustrated using a conducting one-dimensional system. Periodic boundary condition calculations (PBC) were used to perform a HF calculation on a metallic (6,6) single walled carbon nanotube. The PBC code implemented in the *Gaussian* suite of programs [16] calculates the HF exchange in real space as the sum over all significant interactions between a central reference cell and its neighbors (see Appendix B.2).

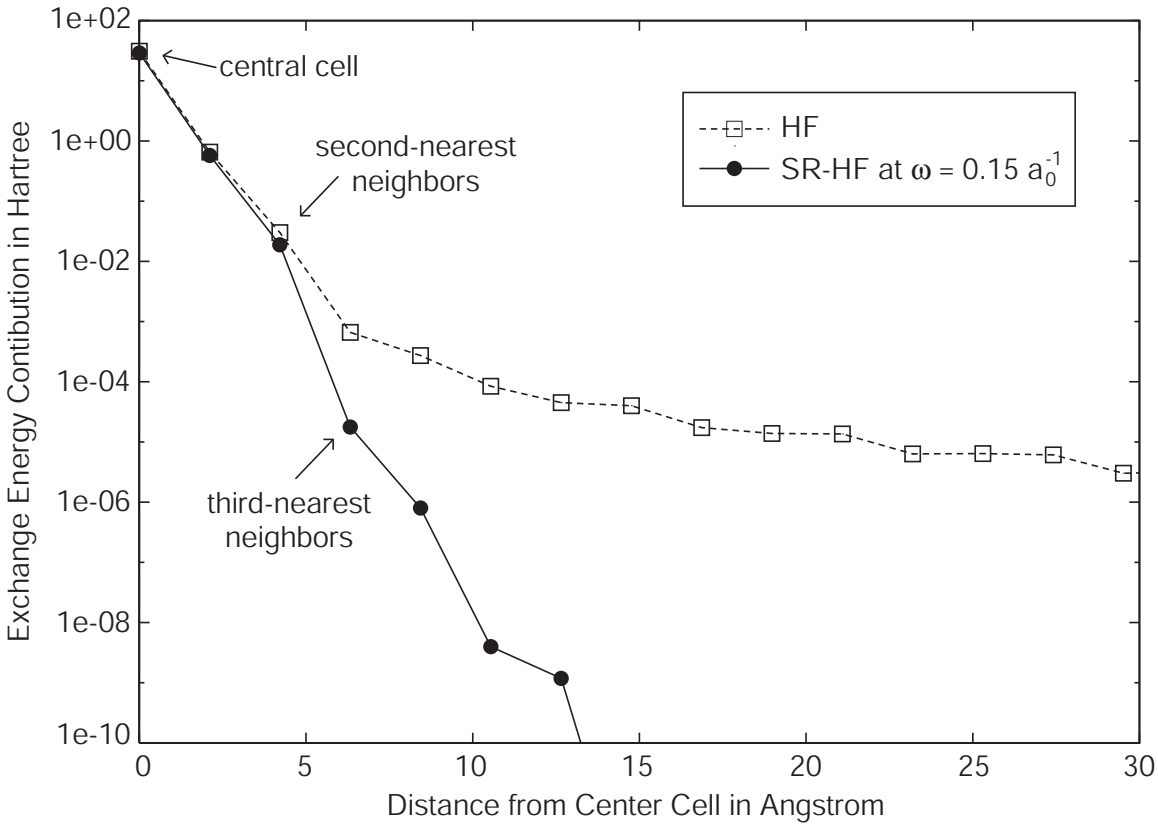

Figure 1.1 : Comparison of decay properties of unscreened (traditional) and short-range HF exchange in a metallic (6,6) carbon nanotube. Exchange energy contribution of a cell vs. its distance from the central (reference) cell.

Figure 1.1 shows the spatial decay of the exchange interactions. The squares depict the HF exchange energy contribution of a given cell as a function of distance from the reference cell. As mentioned above, convergence with distance is very slow in metallic systems and full convergence of HF calculations is extremely hard to achieve. The screened exchange energy contributions (circles) decay exponentially as a function of distance, even though the system has no band gap. In insulators (not shown here), the already present exponential decay is accelerated even further.

In the following chapters, we will first develop a screened Coulomb hybrid functional and discuss its efficient implementation. Then, we turn to an extensive assessment of this functional on small molecules. The examined properties include atomic energies, enthalpies of formation, optimized geometries, vibrational frequencies, ionization potentials, electron affinities, and charge transfers. Finally, the performance of the functional for infinite three-dimensional solids is evaluated. Here, we will focus on lattice constants, bulk moduli, and band gaps. In addition, CPU time requirements for these solids will be presented and compared to traditional hybrid functionals. The details of all these calculations can be found in Appendix B.

Chapter 2

A screened Coulomb potential hybrid functional

We propose a new hybrid functional which performs the exact exchange mixing only for short range interactions in both HF and DFT. This allows the DFT exchange hole to become delocalized among the near neighbors of a reference point, but not beyond.

As a starting point, we use the PBE0 hybrid functional [17, 18, 19, 20], which is based on the Perdew-Burke-Ernzerhof (PBE) exchange-correlation functional [21]. PBE0 assumes the following form for the exchange-correlation energy:

$$E_{\mathrm{xc}}^{\mathrm{PBE0}} = aE_{\mathrm{x}}^{\mathrm{HF}} + (1-a)E_{\mathrm{x}}^{\mathrm{PBE}} + E_{\mathrm{c}}^{\mathrm{PBE}} \tag{2.1}$$

where the mixing coefficient $a = 1/4$ is determined by perturbation theory [17]. We now focus on the expression for the exchange energy

$$E_{\mathrm{x}}^{\mathrm{PBE0}} = aE_{\mathrm{x}}^{\mathrm{HF}} + (1-a)E_{\mathrm{x}}^{\mathrm{PBE}} \tag{2.2}$$

and split all terms into their short and long range components:

$$E_x^{\mathrm{PBE0}} = aE_{\mathrm{x}}^{\mathrm{HF,SR}}(\omega) + aE_{\mathrm{x}}^{\mathrm{HF,LR}}(\omega) + (1-a)E_{\mathrm{x}}^{\mathrm{PBE,SR}}(\omega) + E_{\mathrm{x}}^{\mathrm{PBE,LR}}(\omega) - aE_{\mathrm{x}}^{\mathrm{PBE,LR}}(\omega) \tag{2.3}$$

Numerical tests based on realistic ω values (eg, $\omega = 0.15$ as in Fig. 1.1) indicate that the HF and PBE long range exchange contributions to this functional are rather small (only a few percent), and that these terms tend to cancel each other. Neglecting these terms, we obtain the Heyd-Scuseria-Ernzerhof [9] (HSE) screened Coulomb potential hybrid density functional of the form:

$$E_{\mathrm{xc}}^{HSE} = aE_{\mathrm{x}}^{\mathrm{HF,SR}}(\omega) + (1-a)E_{\mathrm{x}}^{\mathrm{PBE,SR}}(\omega) + E_{\mathrm{x}}^{\mathrm{PBE,LR}}(\omega) + E_{\mathrm{c}}^{\mathrm{PBE}} \tag{2.4}$$

where ω is an adjustable parameter governing the extent of short range interactions. The HSE hybrid functional is equivalent to PBE0 for $\omega = 0$ and asymptotically reaches PBE for $\omega \to \infty$. A derivation of the various short and long range terms in (2.4) is outlined in the following sections.

2.1 Screened Coulomb Potential Hartree-Fock Exchange

The short range component of the HF exchange can be obtained by using the SR Coulomb potential when calculating the electron repulsion integrals (ERI) for the HF

exchange energy [22, 23]. The PRISM algorithm [24] can be modified to generate the short range ERI

$$(\mu\nu|\lambda\sigma)^{\mathrm{SR}} = \iint d\mathbf{r}_1\, d\mathbf{r}_2 \;\; \phi_\mu(\mathbf{r}_1)\phi_\nu(\mathbf{r}_1)\frac{\mathrm{erfc}(\omega r_{12})}{r_{12}}\phi_\lambda(\mathbf{r}_2)\phi_\sigma(\mathbf{r}_2) \tag{2.5}$$

over contracted Gaussian-type basis functions $\phi_i(\mathbf{r})$. It is only necessary to modify the fundamental $[0]^{(m)}$ integrals, from which the ERIs are generated by recursion:

$$[0]^{(m),\mathrm{SR}} = U\left[(2\theta^2)^{m+1/2}G_m(T) - (2\theta_\omega^2)^{m+1/2}G_m(T_\omega)\right] \tag{2.6}$$

where

$$G_m(T) = (2/\pi)^{1/2} \int_0^1 dt\; t^{2m}\exp(-Tt^2)$$

$$\theta^2 = \left(\frac{1}{\zeta}+\frac{1}{\eta}\right)^{-1} \qquad T = \theta^2 R^2$$

$$\theta_\omega^2 = \left(\frac{1}{\zeta}+\frac{1}{\eta}+\frac{1}{\omega^2}\right)^{-1} \qquad T_\omega = \theta_\omega^2 R^2$$

and U, R, ζ and η are derived from the basis functions via the Gaussian product rule (see Ref. [24]). Evaluating the short range ERIs is only slightly more time consuming than the regular ERIs since only the primitive $[0]^{(m)}$ integrals are modified. The contraction and transformation steps of the PRISM algorithm dominate the computational time and remain unchanged.

2.2 A Screened Coulomb Potential

PBE Exchange Functional

The starting point for our screened Coulomb exchange functional is the exchange hole formulation of the PBE functional by Ernzerhof et al. (see Ref. [25] for a detailed description). The PBE exchange energy is defined as an integral over the exchange energy density

$$E_{\mathrm{x}}^{PBE} = \int d\mathbf{r}\ \rho(\mathbf{r})\epsilon_{\mathrm{x}}^{PBE}(\rho(\mathbf{r}), s(\mathbf{r})) \tag{2.7}$$

The energy density $\epsilon_{\mathrm{x}}^{PBE}$ depends on the electron density $\rho(\mathbf{r})$ and the reduced gradient $s = |\nabla\rho|/(2k_F\rho)$ with $k_F = (3\pi^2\rho)^{1/3}$. $\epsilon_{\mathrm{x}}^{PBE}$ is defined as a product of the LDA exchange energy density and an enhancement factor $F_{\mathrm{x}}^{\mathrm{PBE}}$ which depends on the reduced gradient of the electron density:

$$\epsilon_{\mathrm{x}}^{\mathrm{PBE}}(\rho(\mathbf{r}), s(\mathbf{r})) = \epsilon_{\mathrm{x}}^{\mathrm{LDA}}(\rho(\mathbf{r})) \times\ F_{\mathrm{x}}^{\mathrm{PBE}}(s(\mathbf{r})) \tag{2.8}$$

Whereas the original, energy-based, PBE functional uses an explicitly defined enhancement factor, the exchange-hole based formulation defines $F_{\mathrm{x}}^{\mathrm{PBE}}$ as an integral over the PBE exchange hole $J^{\mathrm{PBE}}(s, y)$:

$$F_{\mathrm{x}}^{PBE}(s) = -\frac{8}{9}\int_0^\infty dy\ yJ^{\mathrm{PBE}}(s, y) \tag{2.9}$$

A detailed description of the PBE exchange hole and its derivation is given in Ref. [25].

The short range PBE exchange energy is defined the same way, except that the exchange hole itself is screened by employing the short range Coulomb potential defined in (1.2):

$$J^{\omega\mathrm{PBE,SR}}(\rho, s, y) = J^{\mathrm{PBE}}(s, y) \times \mathrm{erfc}\left(\frac{\omega y}{k_{\mathrm{F}}}\right) \tag{2.10}$$

This formulation introduces an electron density dependence into both the exchange hole and the enhancement factor. The SR exchange hole has the form

$$\begin{aligned} J^{\omega\mathrm{PBE,SR}}(\rho, s, y) = \Bigg[& -\frac{\mathcal{A}}{y^2}\frac{1}{1+(4/9)\mathcal{A}y^2} \\ & + \left(\frac{\mathcal{A}}{y^2} + \mathcal{B} + \mathcal{C}[1+s^2\mathcal{F}(s)]y^2 \right. \\ & \left. + \mathcal{E}[1+s^2\mathcal{G}(s)]y^4\right)\exp(-\mathcal{D}y^2)\Bigg] \\ & \times \exp[-s^2\mathcal{H}(s)y^2] \times \mathrm{erfc}\left(\frac{\omega y}{k_{\mathrm{F}}}\right) \end{aligned} \tag{2.11}$$

where $\mathcal{A} - \mathcal{H}$ are parameters and parametrized functions of the PBE exchange hole. These parameters are not empirical but derived from the functional form of the original, exchange-energy-based PBE functional.

The ωPBE long range exchange contribution is then defined as the integral over the difference of the exchange hole based PBE and the SR ωPBE exchange energy

densities:

$$E_{\mathrm{x}}^{\omega\mathrm{PBE,LR}} = \int d\mathbf{r}\ \rho(\mathbf{r}) \Big[\epsilon_{\mathrm{x}}^{\mathrm{PBE}}(\rho(\mathbf{r}), s(\mathbf{r})) - \epsilon_{\mathrm{x}}^{\omega\mathrm{PBE,SR}}(\rho(\mathbf{r}), s(\mathbf{r})) \Big] \tag{2.12}$$

The following section describes the derivation of the ωPBE enhancement factor in detail.

2.2.1 The ωPBE enhancement factor

The integral over the short range exchange hole, which yields the enhancement factor $F_{\mathrm{x}}^{\omega\mathrm{PBE}}$, cannot be solved analytically due to the terms in (2.11) which contain y in the denominator. Therefore, we chose to use an approximation for the error function which allows the integral to be solved (see below). The approximation is designed to recover the LDA limit of the uniform electron gas by allowing the enhancement factor $F_{\mathrm{x}}^{\omega\mathrm{PBE}}$ to become identical to one for $\omega = s = 0$. In addition, $F_{\mathrm{x}}^{\omega\mathrm{PBE}}$ also satisfies the Lieb–Oxford bound (Section 2.2.3) which the original PBE satisfies, but which is violated in the exchange-hole based PBE.

Let us now take a closer look at the error function and the Lieb–Oxford bound.

2.2.2 Approximating the Error Function

The complementary error function is defined as

$$\mathrm{erfc}(x) = \frac{2}{\sqrt{\pi}} \int_x^\infty e^{-t^2} dt \tag{2.13}$$

This integral does not have a closed-form solution. Therefore, $\mathrm{erfc}(x)$ is usually approximated numerically by a function of the form

$$\mathrm{erfc}(x) \approx P_n(t)\, e^{-x^2} \tag{2.14}$$

where $t = 1/(1 + px)$. The coefficients of $P_n(t)$ as well as p are fitted to the true complementary error function [26]. Various fits use polynomials of orders ranging from four to six. For highly accurate approximations, several such fits over sub-intervals are often used. In the present case, the rational form of t again precludes the analytical evaluation of Eq. (2.9). We use a slightly simplified version of (2.14) instead:

$$\mathrm{erfc}(x) \approx P_8(x)\, e^{-bx^2} \tag{2.15}$$

A higher (8^{th}) order polynomial gives more accurate results in this case since the functional form of (2.15) is inferior to (2.14). This approximation is accurate to 10^{-6} in the interval $0 \leq x \leq 14$ and the resulting exchange hole can be integrated

analytically. The final form of the chosen approximation is

$$\begin{aligned}\operatorname{erfc}(x) \approx (1 + a_1 x + a_2 x^2 + a_3 x^3 + a_4 x^4 + a_5 x^5 \\ + a_6 x^6 + a_7 x^7 + a_8 x^8)\, e^{-bx^2}\end{aligned} \tag{2.16}$$

where the following parameters were fitted via the least-squares method:

$$\begin{aligned} a_1 &= -1.128\,223\,947 & a_2 &= 1.452\,736\,266 \\ a_3 &= -1.243\,162\,299 & a_4 &= 0.971\,824\,836 \\ a_5 &= -0.568\,861\,080 & a_6 &= 0.246\,880\,515 \\ a_7 &= -0.065\,032\,364 & a_8 &= 0.008\,401\,793 \end{aligned}$$

$$b = 1.455\,915\,450$$

For $x > 14$, Eq. (2.9) exhibits numerical instabilities when evaluated using the approximation (2.16). However, in this range the Gaussian term becomes dominant and a much simpler approximation can be used:

$$\operatorname{erfc}(x > 14) \approx e^{-2x^2} \tag{2.17}$$

Additional numerical approximations are necessary to ensure numerical stability over all possible values of the electron density and its gradient. All these approxima-

tions are accurate to better than 10^{-10} and are not discussed in detail here. They can, however, be found in the reference implementation of the ωPBE enhancement factor in Appendix A.

In general, all numerical approximations employed in the ωPBE functional achieve an accuracy much higher than the underlying exchange-hole based implementation of PBE. The PBE exchange hole was fitted to the original PBE functional by Ernzerhof et al. [25] and produces errors in the order of 0.5% in the enhancement factor, compared to PBE.

2.2.3 The Lieb–Oxford Bound

Lieb and Oxford [27] derived a theoretical bound for the maximum value of the exchange-correlation energy E_{xc}. The PBE exchange functional enforces the Lieb-Oxford (L–O) bound

$$E_{\mathrm{x}} \geq -1.679 \int d\mathbf{r} \rho(\mathbf{r})^{4/3} \tag{2.18}$$

by ensuring that the enhancement factor F_{x} satisfies

$$F_{\mathrm{x}}(s) \leq 1.804 \tag{2.19}$$

The exchange-hole based formulation of PBE violates this bound. For the ωPBE functional, we can recover this bound in a straightforward manner.

The L–O bound is not satisfied for reduced gradients $s > 8.57$. This is beyond the

range of s in regions of the electron density relevant to molecules. However, the L–O bound can easily be enforced by smoothly rescaling s beyond a threshold $s_{thresh} > 8.3$. The rescaling is performed by

$$s_{new} = s_{max} - \frac{c}{s^2} \tag{2.20}$$

where $s_{max} = 8.572844$ and $c = 18.796223$. These values ensure the same maximum enhancement factor $F_{\mathrm{x}}(s)$ as the original, energy-based, PBE functional.

In practice, enforcing the Lieb-Oxford bound in the ωPBE functional only changes the exchange energies by less than a mHartree for all examined systems.

2.3 Screening the short range HF exchange integrals

To take advantage of the rapid decay of short range exchange integrals, pre-screening of integral batches is necessary. Both screening methods described below are based on existing bounds and estimates for the contribution of a given batch of integrals to the Fock matrix. The effect of small density matrix elements is also included by multiplying the estimated integral with the largest density matrix element which is contracted with the integral to form an element of the Fock matrix. The present work utilizes two different screening techniques. Compared to traditional hybrid functionals, the combination of SR HF exchange and efficient screening can reduce both computational time and memory requirements drastically.

2.3.1 Schwarz screening

Schwarz screening is an integral part of almost any direct SCF calculation [28] and can easily be modified to account for the SR exchange integrals. Substituting the SR integrals in place of the $1/r$ integrals yields an upper bound of the form:

$$\left|(\mu\nu|\lambda\sigma)_{SR}\right| \leq \sqrt{(\mu\nu|\mu\nu)_{SR}} \cdot \sqrt{(\lambda\sigma|\lambda\sigma)_{SR}} \tag{2.21}$$

The $(ij|ij)_{SR}$ integrals are then evaluated for each batch of integrals and only batches with non-negligible contributions are used in calculating the HF exchange. The SR screening integrals are evaluated by the same procedure as the SR exchange integrals (Section 2.1).

2.3.2 Distance-based multipole screening

Modern quantum chemistry codes employ fast multipole methods (FMM) [29, 30, 31, 32] to efficiently evaluate Coulomb interactions in large molecules and solids. While FMMs cannot be used to evaluate the exchange interaction in an economical manner, multipole moments still provide valuable information about the magnitude of exchange integrals. Multipole moments can be exploited for a distance-based screening scheme of the exchange interactions. The following screening criterion is implemented

in the *Gaussian* suite of programs [16, 33]:

$$T_n = \sum_{M\in\mu\nu}\sum_{M\in\lambda\sigma} C_{\mu\nu}^{\max}\frac{1}{r^{1+M_{\mu\nu}^{\text{low}}+M_{\lambda\sigma}^{\text{low}}}}C_{\lambda\sigma}^{\max} \tag{2.22}$$

where T_n is an estimate for the contribution of a shell quartet and M is a multipole in the multipole expansion of a given shell pair. M_{ij}^{low} are the lowest order multipoles which can contribute to the integral and $C_{ij}^{\max}$ are the maximum coefficients in each order of multipoles. Replacing the $1/r$ potential with the $\text{erfc}(\omega r)/r$ short range potential yields

$$T_n^{SR} = \sum_{M\in\mu\nu}\sum_{M\in\lambda\sigma} C_{\mu\nu}^{\max}\frac{\text{erfc}(\omega r^{1+M_{\mu\nu}^{\text{low}}+M_{\lambda\sigma}^{\text{low}}})}{r^{1+M_{\mu\nu}^{\text{low}}+M_{\lambda\sigma}^{\text{low}}}}C_{\lambda\sigma}^{\max} \tag{2.23}$$

This provides a distance-based upper bound for the SR exchange contribution of a given shell quartet.

2.3.3 Screening efficiency

The implementation of periodic boundary conditions (PBC), used in this work, relies on evaluating all terms of the Hamiltonian in real space [34]. The HF exchange is evaluated using replicated density matrices. All interactions within a certain radius from a central reference cell are calculated and the rest are neglected [35]. This approach works reasonably well for insulating solids since the corresponding density matrix elements decay rapidly. In systems with smaller band gaps, however, the spa-

tial extent of non-negligible contributions to the exchange energy is large. This large extent results in a vast number of significant interactions. To render the computation tractable, the truncation radius must be decreased. Thus, significant interactions are neglected which leads to errors in the total energy of the system and introduces instabilities into the self-consistent field procedure.

Screened Coulomb hybrid functionals do not need to rely on the decay of the density matrix to allow calculations in extended systems. The SR HF exchange interactions decay rapidly and without noticeable dependence on the band gap of the system. The screening techniques, developed above, do not rely on any truncation radius and provide much better control over the accuracy of a given calculation. In addition, the thresholds can be set very tightly, without resulting in extremely long calculations.

A series of benchmark calculations on a three-dimensional system demonstrates the effectiveness of the screening techniques outlined above. Figure 2.1 shows the results for hybrid DFT calculations using both PBE0 and HSE for 3-D silicon (diamond structure). The use of a 6-21G basis set reduced both the computational cost and the convergence problems of the PBE0 calculations. The time per SCF cycle is given as a function of the distance up to which exchange interactions were included in the calculation. As this radius grows, the number of replicated cells grows as $\mathcal{O}(N^3)$. The PBE0 curve tracks this growth since regular HF exchange has a large spatial extent. The relatively small band gap of silicon (1.9 eV in this calculation) is insufficient for

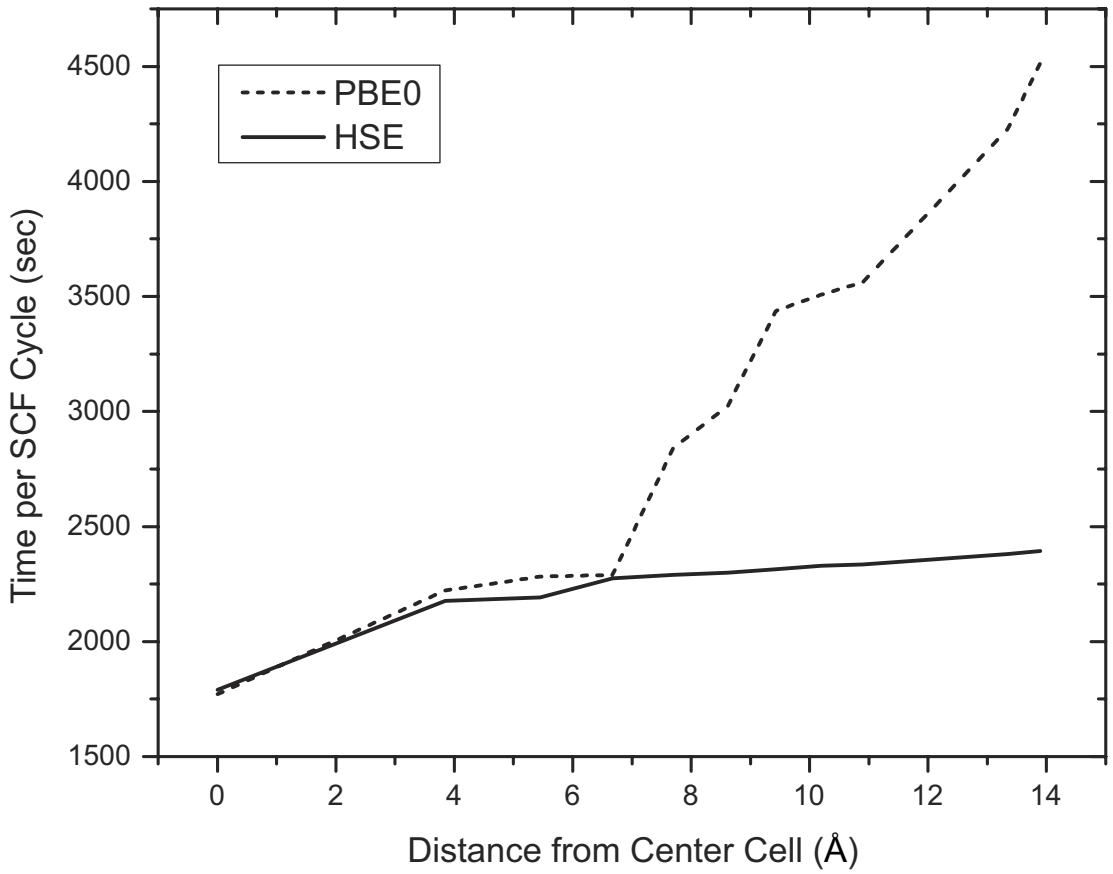

Figure 2.1 : Si/6-21G: Comparison of the CPU time scaling behavior of the traditional PBE0 hybrid functional and the HSE screened Coulomb hybrid.

density matrix elements to decay noticeably. HSE, on the other hand, only shows a modest increase in CPU time as the system becomes larger. Beyond 10 Å, the CPU time only increases due to the time spent on screening.

Figure 2.2 shows the convergence of the total energy in the same silicon crystal. The HSE calculation converges very rapidly and only cells up to 10 Å from the reference cell contribute to the exchange energy. PBE0, by comparison, converges significantly slower. Thus HSE not only reduces the CPU time drastically, but also

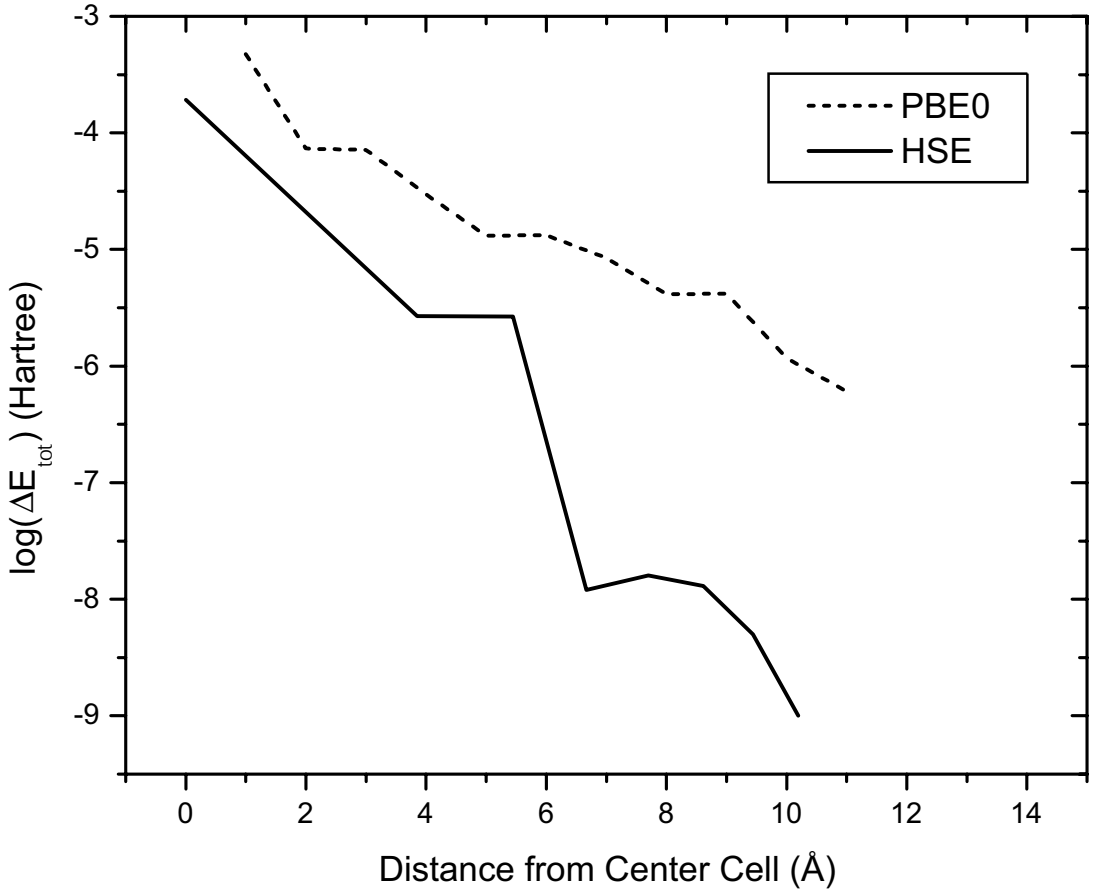

Figure 2.2 : Si/6-21G: Comparison of the spatial convergence of the exchange interactions of the traditional PBE0 hybrid functional and the HSE screened Coulomb hybrid.

decreases the memory requirements of a given calculation since less replicated density matrices need to be stored in memory. In practice, HSE calculations can be performed with the same amount of memory as pure DFT calculations, whereas traditional hybrid methods have larger memory demands.

The following chapters present a detailed assessment of the HSE functional on both molecules and solids.

Chapter 3

Atomic and molecular calculations

Given the HSE functional developed in the previous chapter, we now apply it to calculations of atoms and molecules. First, the screening (ω) and mixing (a) parameters are examined. Then, we move on to atomic calculations and finally the HSE functional is assessed on a wide range of molecules and its performance is compared to the established B3LYP [3], PBE [21] and PBE0 [19] functionals. We present results for enthalpies of formation, geometry optimizations, vibrational frequencies, ionization potentials, electron affinities and charge transfers in a variety of molecules. While only summarized results are shown in this chapter, detailed results for the HSE functional can be found in Appendix C.

3.1 Determining the screening and mixing parameters

To validate our approach in Chapter 2, we compare the new HSE functional to a PBE0-like hybrid which uses the screened SR HF exchange instead of the full HF exchange:

$$E_{\rm xc}^{\text{SR-HF PBE0}} = aE_{\rm x}^{\rm HF,SR} + (1-a)E_{\rm x}^{\rm PBE} + E_{\rm c}^{\rm PBE} \tag{3.1}$$

where $a = 1/4$. Mean absolute errors (MAE) for standard enthalpies of formation at 298K were calculated as a function of ω. Results for the G2-1 set of 55 small

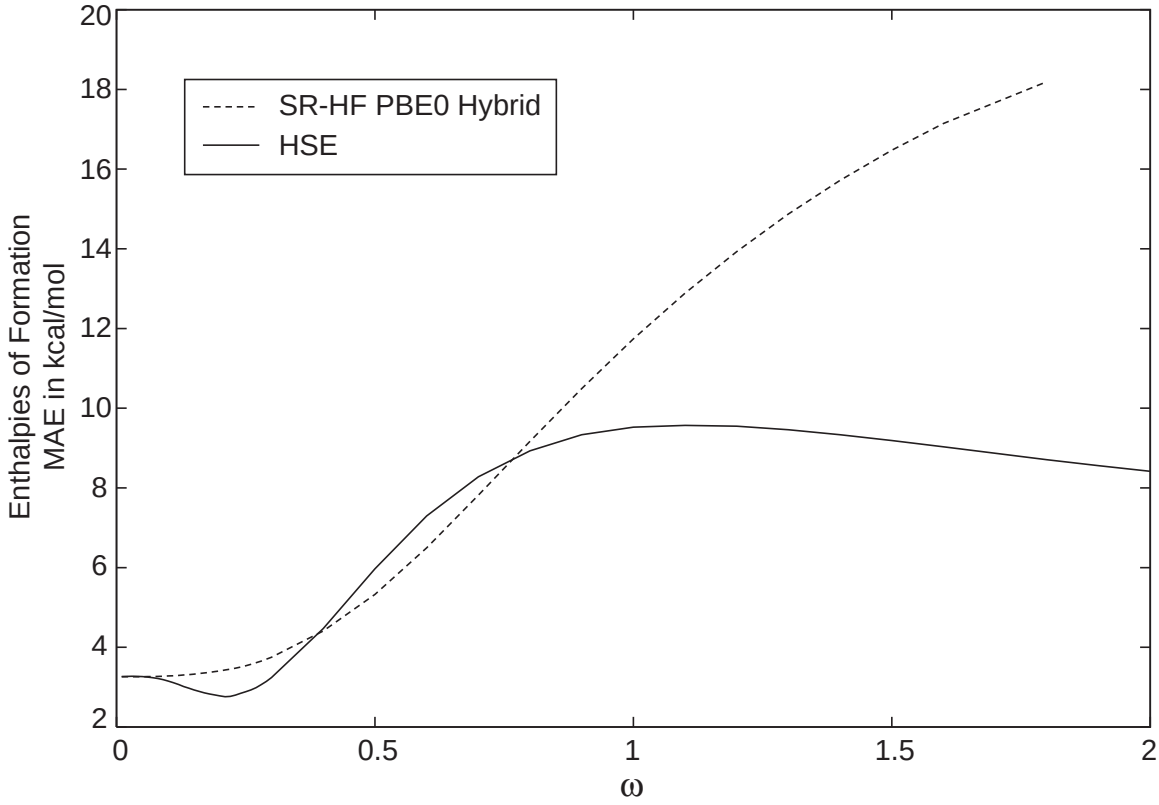

Figure 3.1 : Mean absolute error in standard enthalpies of formation of the G2-1 set (55 molecules): SR-HF PBE0 Hybrid compared to HSE as a function of ω

molecules [36] are shown in Figure 3.1. For $\omega = 0$, HSE reproduces PBE0 (up to a slight deviation due to the parametrization of the PBE exchange hole). HSE reduces to the non-hybrid PBE functional for $\omega \to \infty$. The computational effort necessary to calculate the SR HF exchange decreases drastically with increasing ω.

An extensive study of the ω-dependence of various properties was performed for both molecules and solids. All calculated molecular properties only show a very slight dependence on ω in the range from $\omega = 0.05$ to $0.35\ a_0^{-1}$, which validates our earlier assumption. In order to reproduce reliable values for the band gap in semiconducting

solids, it is necessary to choose $\omega \leq 0.15$. In these systems, the calculated band gap is directly proportional to the HF contribution to the exchange energy.

In addition, two dimensional optimizations of both a and ω were carried out over the G2-1 set of small molecules and for selected periodic systems. The minima in parameter space were very broad and give no reason to change the mixing coefficient $a = 1/4$.

A balanced description that provides good accuracy and speed, both in molecules and solids, can be achieved by choosing $\omega = 0.15\ a_0^{-1}$. This value will be used hereafter.

3.2 Atomic energies

Table 3.1 shows the total energies for the H-Ne atoms, comparing the new HSE functional to PBE and PBE0. The modest underestimation of the total energies is due to different decay properties of HF and DFT exchange energy potentials. The more delocalized SR-HF exchange falls off slightly slower for $\omega > 0$ than the LR-DFT exchange increases. This produces a slight overall increase in the exchange energy, due to an overcompensation by the LR-DFT part. In addition, the lack of self-interaction correction in the PBE correlation functional contributes to the underestimation of the total energies.

Table 3.1 : Total non-relativistic energies of atoms (Hartree)[a]

Atom	Exact[b]	PBE	PBE0	HSE
H	−0.500	−0.500	−0.501	−0.511
He	−2.904	−2.891	−2.894	−2.916
Li	−7.478	−7.460	−7.466	−7.496
Be	−14.667	−14.628	−14.635	−14.676
B	−24.654	−24.609	−24.617	−24.672
C	−37.845	−37.794	−37.803	−37.871
N	−54.589	−54.529	−54.540	−54.621
O	−75.067	−75.005	−75.013	−75.107
F	−99.734	−99.661	−99.667	−99.775
Ne	−128.938	−128.846	−128.851	−128.971

[a]6-311++G(3df,3pd) basis set
[b]Exact atomic energies from Ref. [37]

3.3 Standard enthalpies of formation

The G3/99 set of 223 small molecules [36, 38] was used to assess the performance for predicting standard enthalpies of formation. Results for two subsets of the G3 set, the G2-1 (55 molecules) and G2-1+G2-2 (148 molecules, denoted G2) sets, are presented as well since a large amount of data for these test sets exists in the literature.

The HSE and PBE0 functionals exhibit similar performance with HSE producing slightly better results. The mean absolute errors (MAE) of HSE are 2.89 kcal/mol, 4.64 kcal/mol and 6.57 kcal/mol for the G2-1, G2 and G3 sets, respectively. The errors for PBE0 are 3.01 kcal/mol, 5.15 kcal/mol and 7.29 kcal/mol. On all three test sets, the B3LYP functional yields the best results. The MAEs are 2.46 kcal/mol,

3.04 kcal/mol and 4.31 kcal/mol for the G2-1, G2 and G3 sets, respectively. The non-hybrid PBE functional produces errors which are 4-6 times larger than any of the tested hybrid functionals (8.19 kcal/mol, 17.19 kcal/mol and 22.88 kcal/mol). Table 3.2 shows a summary of the results.

While neither HSE nor PBE0 yield accuracy comparable to B3LYP, the latter functional contains empirical parameters which were optimized on the G2-1 set of molecules. PBE0 does not contain any empirical parameters, and HSE employs only the short-range / long-range splitting parameter $\omega = 0.15$. The dependence on ω is fairly small (see Section 3.1) and while ω has been chosen to give good results for the G2-1 set, it does not represent a fully optimized empirical parameter.

To estimate the effect of the molecular geometries, the 148 molecules in the G2-1 and G2-2 test sets were re-optimized with the individual functionals (instead of using the MP2 optimized geometries). The enthalpies of formation predicted in this case (Table 3.3), all exhibit errors within 0.25 kcal/mol of the calculations using MP2 geometries. This agreement is no surprise since geometry optimizations using any of the above functionals yield excellent accuracy, as shown in the next section.

Table 3.2 : Summary of results for enthalpies of formation at MP2 optimized geometries (kcal/mol).[a]

	G2-1 Set[b]			
Method	MAE[e]	RMS[f]	Max.(−)[g]	Max.(+)[h]
B3LYP	2.46	3.28	−8.2	9.9
PBE	8.19	10.40	−29.1	10.1
PBE0	3.01	3.76	−6.1	10.6
HSE	2.89	3.70	−7.3	10.3
	G2-1 and G2-2 Set[c]			
Method	MAE	RMS	Max.(−)	Max.(+)
B3LYP	3.04	4.40	−8.2	20.0
PBE	17.19	21.00	−50.8	10.1
PBE0	5.15	6.78	−20.8	21.7
HSE	4.64	6.21	−19.3	20.0
	Complete G3 Set[d]			
Method	MAE	RMS	Max.(−)	Max.(+)
B3LYP	4.31	5.83	−8.2	21.0
PBE	22.88	27.71	−83.3	10.1
PBE0	7.29	9.75	−37.9	21.7
HSE	6.57	8.90	−35.5	20.0

[a]6-311++G(3df,3pd) basis
[b]55 molecules
[c]148 molecules
[d]223 molecules
[e]Mean absolute error
[f]Root mean square error
[g]Maximum negative deviation
[h]Maximum positive deviation

Table 3.3 : Summary of results for enthalpies of formation at geometries optimized with each functional (kcal/mol).[a]

	G2-1 Set[b]			
Method	MAE[d]	RMS[e]	Max.(−)[f]	Max.(+)[g]
B3LYP	2.33	3.07	−8.2	7.7
PBE	8.33	10.60	−29.2	10.0
PBE0	2.79	3.43	−6.1	9.8
HSE	2.73	3.37	−7.3	9.5
	G2-1 and G2-2 Set[c]			
Method	MAE	RMS	Max.(−)	Max.(+)
B3LYP	2.99	4.29	−8.2	19.8
PBE	17.40	21.24	−50.8	10.0
PBE0	5.35	6.92	−21.2	21.1
HSE	4.86	6.31	−19.8	19.4

[a] 6-311++G(3df,3pd) basis
[b] 55 molecules
[c] 148 molecules
[d] Mean absolute error
[e] Root mean square error
[f] Maximum negative deviation
[g] Maximum positive deviation

Table 3.4 : Summary of results for bond length optimization of the 96 diatomic molecules, radicals and ions in the T-96R set [5] (Å).

	6-311++G(3df,3pd) basis set			
Method	MAE[a]	RMS[b]	Max.(−)[c]	Max.(+)[d]
B3LYP	0.010	0.014	−0.040	0.041
PBE	0.016	0.019	−0.013	0.055
PBE0	0.010	0.015	−0.052	0.063
HSE	0.009	0.013	−0.050	0.039
	6-31G* basis set			
Method	MAE	RMS	Max.(−)	Max.(+)
B3LYP	0.020	0.025	−0.041	0.074
PBE	0.028	0.032	−0.019	0.078
PBE0	0.015	0.020	−0.038	0.080
HSE	0.014	0.018	−0.040	0.057

[a]Mean absolute error
[b]Root mean square error
[c]Maximum negative deviation
[d]Maximum positive deviation

3.4 Optimized geometries

To further assess the accuracy of geometry optimizations, the geometries of 96 molecules, radicals and ions of the T-96R [5] set were optimized and compared to experimental bond lengths (see references in [5]). This recently compiled test set contains 86 neutral molecules and 10 molecular cations. It is comprised of diatomic molecules as well as several high-symmetry polyatomics whose geometries are fully defined by a single

bond length.

Using the 6-311++G(3df,3pd) basis set, all three hybrid functionals yield excellent accuracy with a MAE of around 0.010 Å. The pure PBE functional exhibits slightly larger errors (MAE of 0.016 Å). The HSE functional performs slightly better than any of the established functionals which were tested.

In other works, geometry optimizations are usually carried out with the more modest 6-31G* basis set. Using this basis set, the results for the three hybrid functionals are not as uniform as with the larger basis. The MAE of B3LYP increases by 100% to 0.020 Å while the errors of both HSE and PBE0 increase by only 50% to 0.014 Å and 0.015 Å, respectively. Table 3.4 shows a summary of all the results.

3.5 Vibrational frequencies

The recently compiled T-82F set [5] of diatomic molecules, radicals and cations provides a broad range of test systems for the prediction of harmonic vibrational frequencies. Vibrational frequencies, just like geometry optimizations, are usually performed using smaller basis sets. The geometries of all systems in the T-82F set were therefore optimized using both the 6-311++G(3df,3pd) and 6-31G* basis sets and vibrational frequency calculations were performed using the same basis sets. Table 3.5 shows a summary of the results.

HSE is in close agreement with PBE0. Both yield MAEs of 44 cm^{-1} using the large basis set and 47 cm^{-1} with the smaller basis. The PBE functional gives results

Table 3.5 : Summary of results for harmonic vibrational frequencies of the 82 diatomic molecules, radicals and cations in the T-82F set [5] (cm^{-1}).

	6-311++G(3df,3pd) basis set			
Method	MAE[a]	RMS[b]	Max.(−)[c]	Max.(+)[d]
B3LYP	33.5	48.5	−99.2	161.9
PBE	42.0	57.6	−175.3	82.5
PBE0	43.6	66.8	−26.2	236.3
HSE[e]	43.9	66.7	−32.9	236.2

	6-31G* basis set			
Method	MAE	RMS	Max.(−)	Max.(+)
B3LYP	39.5	57.3	−187.8	148.5
PBE	47.7	70.1	−266.2	101.9
PBE0	46.8	70.1	−126.8	230.7
HSE	47.0	70.2	−129.9	230.0

[a]Mean absolute error
[b]Root mean square error
[c]Maximum negative deviation
[d]Maximum positive deviation
[e]Numerical 2^{nd} derivatives from analytic gradients

similar to its hybrid cousins: 42 cm^{-1} and 48 cm^{-1} with the large and small basis sets, respectively. B3LYP outperforms all other functionals in this test with MAEs of 34 cm^{-1} and 39 cm^{-1}. However, as in the geometry optimizations in section 3.4, using a smaller basis set has a significantly larger effect on B3LYP than on the other hybrid functionals.

Table 3.6 : Summary of results for ionization potentials of 86 molecules of the G3 set (eV).

Method	MAE[a]	RMS[b]	Max.(−)[c]	Max.(+)[d]
B3LYP	0.176	0.261	−0.56	1.59
PBE	0.220	0.291	−1.15	0.45
PBE0	0.197	0.273	−0.67	1.63
HSE	0.227	0.348	−0.39	1.99

[a]Mean absolute error
[b]Root mean square error
[c]Maximum negative deviation
[d]Maximum positive deviation

3.6 Ionization potentials and electron affinities

The performance of the HSE functional for ionization potentials (IPs) and electron affinities (EAs) was examined using the G2/97 ion test set [39]. The calculations of the H_2S^+ and N_2^+ cations do not converge with pure DFT methods [39] and these two species were dropped from the test set. Our test set thus comprised 86 ionization potentials and 58 electron affinities. Geometry optimizations of all ions and neutral molecules were performed with each tested functional using the 6-311++G(3df,3pd) basis set. Both IPs and EAs were calculated as the difference in energy of the charged vs. the neutral species at 0K.

For ionization potentials, B3LYP produces the smallest mean absolute error of 0.176 eV, compared to experiment. The MAEs of PBE, PBE0 and HSE are 0.220 eV, 0.197 eV and 0.227 eV, respectively. Table 3.6 shows a more detailed summary

Table 3.7 : Summary of results for electron affinities of 58 molecules of the G3 set (eV).

Method	MAE[a]	RMS[b]	Max.(−)[c]	Max.(+)[d]
B3LYP	0.126	0.213	−0.10	1.10
PBE	0.123	0.171	−0.30	0.78
PBE0	0.163	0.219	−0.38	1.09
HSE	0.210	0.300	−0.11	1.32

[a]Mean absolute error
[b]Root mean square error
[c]Maximum negative deviation
[d]Maximum positive deviation

of the results. As noted in previous studies [39, 5], the errors of all functionals are similar and close to 0.2 eV.

Calculations of electron affinities by density functional methods have sparked discussions whether approximate DFT is a valid approach to calculate EAs [40, 41]. Negative ions are usually unstable when described via not completely self-interaction-free functionals [42]. The success of DFT to predict EAs seems to rest on error cancellation and basis set effects. Nonetheless, we calculated electron affinities using HSE and the three other functionals. The established functionals exhibit MAEs ranging from 0.123 eV for PBE to 0.126 eV and 0.163 eV for B3LYP and PBE0, respectively. The HSE functional produces a slightly larger error of 0.210 eV.

The lower performance of HSE, compared to PBE0, is unexpected given the close agreement of these two functionals for all other examined properties. A closer in-

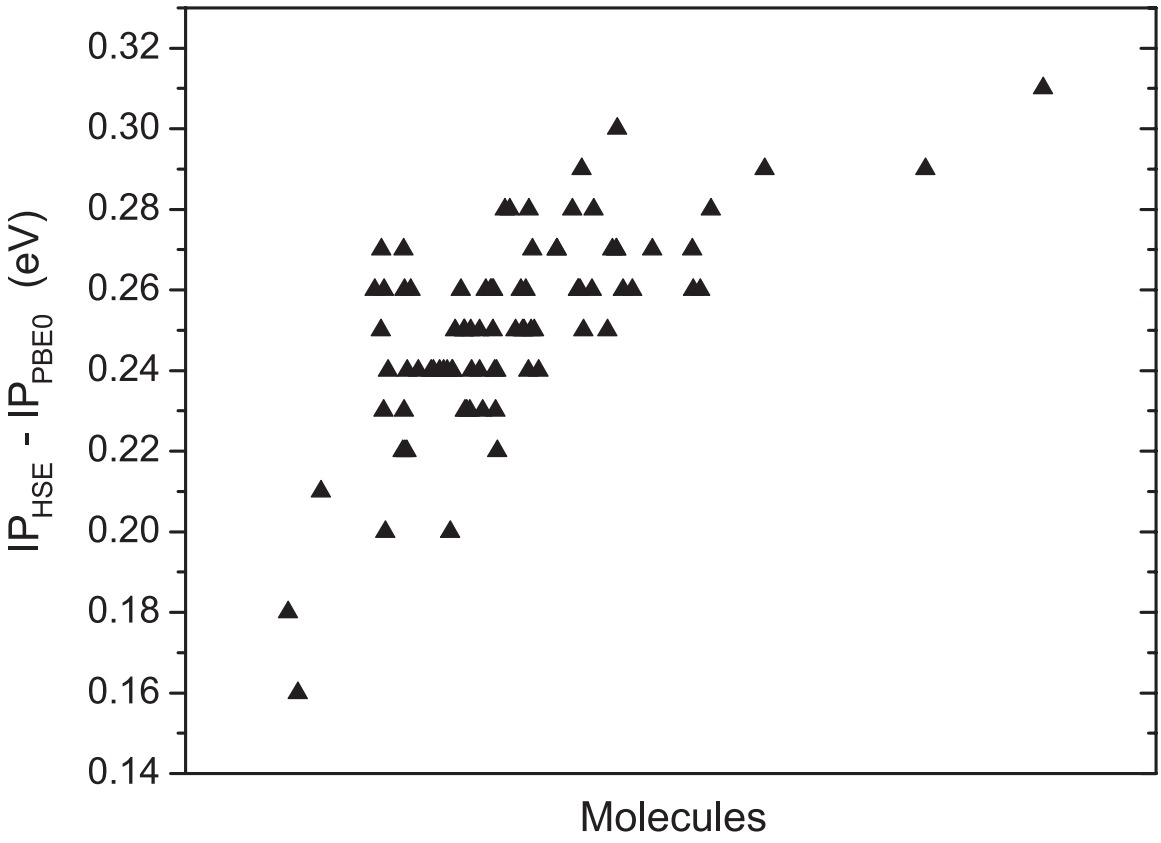

Figure 3.2 : Difference between HSE and PBE0 in predicted ionization potential (eV)

spection of results for individual molecules shows HSE to overestimate both IPs and EAs by 0.23-0.25 eV compared to PBE0. Figure 3.2 shows the distribution of the differences in IPs over the test set. Subtracting 0.24 eV from each IP and EA renders the HSE results virtually identical to the PBE0 results. This shift is independent of the magnitude of the EA or IP and points toward a deficiency in the theoretical model of HSE. The source of this behavior remains uncertain and its origin needs to be investigated further.

Table 3.8 : Transition metal hexacarbonyls: Optimized geometries (Å).[a]

Metal	Bond	B3LYP	PBE	PBE0	HSE	Exp.[b]
Cr	r_{MC}	1.920	1.898	1.892	1.897	1.914
	r_{CO}	1.141	1.155	1.139	1.139	1.141
Mo	r_{MC}	2.007	2.061	2.056	2.060	2.063
	r_{CO}	1.141	1.154	1.139	1.138	1.145
W	r_{MC}	2.083	2.071	2.065	2.068	2.058
	r_{CO}	1.143	1.155	1.140	1.139	1.148
MAE	r_{MC}	0.015	0.010	0.012	0.010	–
	r_{CO}	0.003	0.010	0.005	0.006	–
	total	0.009	0.010	0.009	0.008	–

[a] O_h symmetry, Stuttgart 97 RSC ECP on metal and 6-311G(d) on carbon and oxygen
[b] See [43] and references therein

3.7 Transition metal complexes

DFT methods have always been quite successful in describing molecules and complexes containing transition metals [43]. Therefore, the HSE functional was also tested on a series of transition metal hexacarbonyls. Geometry optimizations of the hexacarbonyls of chromium, molybdenum and tungsten were performed and charge transfer within the complexes was analyzed using natural bond orbital theory.

The optimized geometries of all four functionals are close to experiment (see Table 3.8). HSE gives the best overall agreement with experimental bond lengths (MAE of 0.008 Å). PBE0 and B3LYP are close seconds with MAEs of 0.009 Å, followed by PBE with an error of 0.010 Å. The metal-ligand distance is best described by HSE

Table 3.9 : Transition metal hexacarbonyls: Natural bond orbital derived charges.[a]

Metal	Atom	B3LYP	PBE	PBE0	HSE
Cr	M	-1.357	-1.386	-1.466	-1.445
	C	0.677	0.645	0.695	0.691
	O	-0.451	-0.414	-0.450	-0.451
Mo	M	-1.203	-1.183	-1.281	-1.261
	C	0.641	0.599	0.652	0.649
	O	-0.441	-0.402	-0.438	-0.439
W	M	-0.998	-0.975	-1.076	-1.056
	C	0.602	0.560	0.614	0.611
	O	-0.436	-0.398	-0.434	-0.435

[a] O_h symmetry, optimized geometries from Table 3.8,
Stuttgart 97 RSC ECP on metal and 6-311G(2df) on carbon and oxygen

and PBE (MAE of 0.010 Å), while all three hybrid functionals yield better results for the carbon-oxygen bond lengths than PBE.

No experimental data exists for the partial charges of atoms inside these hexacarbonyl complexes. Nonetheless, examining natural bond orbital (NBO) derived charges is instructive since some general information about the methods can be obtained. The PBE pure DFT functional polarizes bonds less than all three hybrid functionals. HSE gives results similar to PBE0 and B3LYP (Table 3.9). Thus, neglecting the long range HF exchange does not adversely affect the wave function of the calculated system.

Chapter 4

Periodic Boundary Condition Calculations

Given the fast decay of the short range HF interactions and the high screening efficiency shown in Chapter 2, as well as the accurate results obtained for molecules, we then applied HSE to a variety of three-dimensional solids. We examined the predicted lattice constants and bulk moduli of 21 metals, semi-conductors and insulators and compared the results to the established LDA, PBE and TPSS non-hybrid density functional results. In addition, we performed single point calculations for eight semi-conducting systems (at the previously found lattice constants) to assess the prediction of band gaps. The 21 systems were chosen to represent a wide variety of solids. However, we restricted the present assessment to systems with a single lattice constant. This restriction simplifies the determination of lattice constants and bulk moduli considerably. In general, the present assessment closely follows the non-hybrid DFT functional work of Staroverov et al. [6] which also provided most of the experimental results. Table 4.1 lists the 21 chosen systems as well as the basis sets used in the calculations. Further computational details can be found in Appendix B.

Table 4.1 : Structures and basis sets used for the calculation of 21 bulk solids

Solid	Structure	Basis set
Li	A2 (bcc)	[4s,3p,1d][a]
Na	A2 (bcc)	[5s,3p,1d][b]
K	A2 (bcc)	[6s,4p,1d][b]
Al	A1 (fcc)	[6s,3p,1d][c]
BN	B3 (zincblende)	6-31G*
BP	B3 (zincblende)	6-31G*
C	A2 (diamond)	6-31G*
Si	A2 (diamond)	6-31G*
SiC	B3 (zincblende)	6-31G*
β-GaN[d]	B3 (zincblende)	[6s,5p,2d]/[4s,3p][e]
		[7s,6p,3d][f]/[5s,4p,1d][g]
GaP[d]	B3 (zincblende)	[6s,5p,2d]/6-31G*[e]
		[7s,6p,3d][f]/6-31G*
GaAs	B3 (zincblende)	[6s,5p,2d]/6-311G*[e]
LiF	B1 (cubic)	[4s,3p,1d][h]/6-311G*
LiCl	B1 (cubic)	[4s,3p,1d][h]/6-311G*
NaF	B1 (cubic)	[6s,4p,1d][i]/6-311G*
NaCl	B1 (cubic)	[6s,4p,1d][i]/6-311G*
MgO	B1 (cubic)	[4s,3p,1d]/[4s,3p,1d][j]
Cu	A1 (fcc)	[6s,5p,2d][k]
Rh	A1 (fcc)	ECP-[4s,4p,2d][l]
Pd	A1 (fcc)	ECP-[4s,4p,2d][l]
Ag	A1 (fcc)	ECP-[4s,4p,2d][l]

[a]Ref. [44]
[b]Ref. [45]
[c]Ref. [46]
[d]First basis set for structural parameters, second one for band gap calculations
[e]Ref. [47]
[f]Ga: 6-311G* without the most diffuse *s*- and *p*-type functions
[g]Na: 6-311G* plus one additional *sp*-type function with exponent 0.15
[h]Li: 6-311G* with the exponents of the two outer *sp*-functions multiplied by 6
[i]Na: 6-311G* with the exponents of the two outer *s*-functions multiplied by 6, the contraction of two *p*-functions resolved into primitives, and without the two outer *p*-functions
[j]Ref. [48]
[k]Ref. [49]
[l]LANL effective core potentials [49] with the GTO basis from Ref. [50]

Table 4.2 : Lattice constants for 21 solids (Å)

Solid	LDA	PBE	TPSS	HSE	Exp
Li	3.383	3.453	3.475	3.454	3.477
Na	4.049	4.199	4.233	4.166	4.225
K	5.093	5.308	5.362	5.275	5.225
Al	4.008	4.063	4.035	3.991	4.032
BN	3.584	3.629	3.630	3.603	3.616[a]
BP	4.517	4.575	4.575	4.549	4.538[a]
C	3.544	3.583	3.583	3.557	3.567
Si	5.426	5.490	5.477	5.454	5.430
SiC	4.351	4.401	4.392	4.370	4.358
β-GaN	4.452	4.539	4.527	4.498	4.520[b]
GaP	5.377	5.493	5.483	5.455	5.451[a]
GaAs	5.592	5.726	5.702	5.683	5.648
LiF	3.904	4.062	4.026	3.995	4.010
LiCl	4.968	5.148	5.113	5.098	5.106
NaF	4.505	4.700	4.706	4.631	4.609
NaCl	5.471	5.698	5.696	5.638	5.595
MgO	4.156	4.242	4.224	4.200	4.207
Cu	3.530	3.636	3.593	3.631	3.603
Rh	3.791	3.871	3.846	3.838	3.798
Pd	3.851	3.950	3.917	3.932	3.881
Ag	3.997	4.130	4.076	4.129	4.069

[a]Ref. [51]
[b]Ref. [52]

Table 4.3 : Lattice constants for 21 solids (errors, Å)

	All systems			
	LDA	PBE	TPSS	HSE
ME[a]	−0.067	0.046	0.034	0.009
MAE[b]	0.067	0.049	0.035	0.028
RMS[c]	0.083	0.055	0.050	0.033
Std. Dev.[d]	0.049	0.034	0.038	0.032
Max.(−)[e]	−0.176	−0.026	−0.010	−0.059
Max.(+)[f]	–	0.103	0.137	0.060
	Without metals			
	LDA	PBE	TPSS	HSE
ME	−0.062	0.052	0.037	0.006
MAE	0.062	0.048	0.037	0.017
RMS	0.076	0.055	0.048	0.021
Std. Dev.	0.045	0.027	0.031	0.020
Max.(−)	−0.138	–	–	−0.022
Max.(+)	–	0.103	0.101	0.043

[a]Mean error
[b]Mean absolute error
[c]Root mean square error
[d]Standard deviation
[e]Maximum negative deviation
[f]Maximum positive deviation

4.1 Lattice constants

In all the examined solids, the crystal structure is determined by a single lattice constant. Table 4.2 shows the optimal lattice constants found using the Murnaghan equation of state [53]. The accuracy of the predicted values correlates directly with the level of approximation in the functional. HSE gives the most accurate results, followed by the TPSS meta-GGA functional, the PBE GGA functional and finally

LDA. The mean absolute errors (MAE) over the whole test set are 0.028 Å, 0.035 Å, 0.049 Å, and 0.067 Å, respectively.

Metallic systems are usually described well by a pure density functional approach. Semi-conductors and insulators, however, seem to benefit greatly from the portion of exact exchange which is introduced by hybrid functionals. When the results for metallic systems are excluded from the statistics, the MAE of HSE drops to 0.017 Å, whereas the errors for pure density functionals remain virtually the same.

4.2 Bulk moduli

The predictions of bulk moduli are somewhat more sensitive to the functional employed (Table 4.4). LDA tends to overestimate bulk moduli due to the overbinding of individual bonds, resulting in a mean error (ME) of 11.8 GPa. The GGA and meta-GGA functionals reverse this trend, now underestimating the bulk moduli (ME of -9.2 GPa and -4.1 GPa, respectively). The HSE hybrid functional exhibits a significantly smaller ME of 1.4 GPa (Table 4.5). The MAEs also reflect this: 12.6 GPa (LDA), 10.1 GPa (PBE), 9.9 GPa (TPSS) and 4.4 GPa (HSE).

Table 4.4 : Bulk moduli for 21 solids (GPa)

Solid	LDA	PBE	TPSS	HSE	Exp
Li	14.7	13.6	13.2	14.0	13.0
Na	9.1	7.7	7.3	9.9	7.5
K	4.6	3.8	3.6	4.1	3.7
Al	81.8	76.2	84.7	94.4	79.4
BN	397	368	370	398	400[a]
BP	170	158	158	171	165[a]
C	454	422	417	458	443
Si	95.1	88.6	91.5	99.1	99.2
SiC	224	207	211	225	225
β-GaN	214	183	190	207	210[b]
GaP	95.0	80.4	81.3	91.4	88.7[a]
GaAs	81.1	68.0	70.0	76.9	75.6
LiF	86.8	65.4	66.5	74.7	69.8
LiCl	41.8	32.7	34.1	36.3	35.4
NaF	62.8	47.3	43.7	52.2	51.4
NaCl	32.2	23.7	22.9	25.7	26.6
MgO	182	161	168	175	165
Cu	188	150	171	143	142
Rh	303	239	257	262	269
Pd	235	177	200	181	195
Ag	149	106	127	104	109

[a]Ref. [51]
[b]Ref. [52]

Table 4.5 : Bulk moduli for 21 solids (errors, GPa)

	All systems			
	LDA	PBE	TPSS	HSE
ME	11.8	−9.2	−4.1	1.4
MAE	12.6	10.1	9.9	4.4
RMS	18.9	14.0	13.6	6.5
Std Dev	15.1	10.8	13.2	6.5
Max (-)	−4.1	−31.8	−30.5	−13.8
Max (+)	46.0	8.0	29.0	15.2
	Without metals			
	LDA	PBE	TPSS	HSE
ME	6.3	−11.5	−10.1	2.7
MAE	8.1	10.0	9.1	3.6
RMS	9.6	12.7	11.7	5.8
Std Dev	6.6	8.2	8.5	5.3
Max (-)	−4.1	−26.6	−26.0	−3.0
Max (+)	17.0	−2.7	3.0	15.2

When only the semi-conducting and insulating systems are examined, certain parallels to the case of the lattice constants appear. Again, the PBE and TPSS errors remain similar to the errors of the full set of solids. However, the LDA error decreases significantly to 8.1 GPa. Most likely, this improvement is due to a cancellation of errors. As with the lattice constants, the MAE of HSE drops noticeably to 3.6 GPa.

4.3 Band gaps

The calculation of band gaps in solids has always been the Achilles heel of pure density functional methods [54]. Recently, hybrid density functional studies of band gaps [55, 56] have demonstrated that including some HF exchange improves results dramatically. Here, we chose a subset of eight semi-conducting systems to assess the performance of the HSE functional and compare it with pure DFT functionals.

For the gallium compounds, it was necessary to use a larger basis set for band gap calculations than for the structural properties. While the 6-31G* basis set proved sufficient for P, modified versions of 6-311G* were used for Ga and N. (see Table 4.1). A similar treatment is necessary for GaAs. In the present study, however, we excluded GaAs from the band gap calculations since the computational cost of optimizing the basis set becomes rather large.

The results shown in Table 4.6 speak volumes. All pure DFT functionals severely underestimate the band gaps, resulting in MAEs of around 1.3 eV, while HSE produces excellent agreement with experiment (0.24 eV MAE).

Table 4.6 : Band gaps for 8 semi-conductors (eV)

Solid	LDA	PBE	TPSS	HSE	Exp[a]	Type[b]
C	4.13	4.10	4.16	5.43	5.48	I
Si	0.52	0.71	0.78	1.31	1.17	I
BN	4.38	4.45	4.47	5.97	6.4	I
BP	1.23	1.35	1.41	2.15	2.4	I
SiC	1.32	1.39	1.35	2.39	2.42	I
β-GaN	2.24	1.85	1.79	3.48	3.20[c]	D
GaP	1.50	1.79	1.82	2.46	2.35	I
MgO	5.39	4.91	5.20	7.09	7.7[c]	D
ME[d]	-1.30	-1.32	-1.27	-0.10	–	
MAE[e]	1.30	1.32	1.27	0.24	–	
RMS[f]	1.41	1.50	1.43	0.30	–	
Std Dev[g]	0.73	0.82	0.81	0.30	–	
Max $(-)^h$	-2.31	-2.79	-2.50	-0.61	–	
Max $(+)^i$	–	–	–	0.28	–	

[a]All experimental values from Ref. [51] unless noted otherwise
[b]Direct (D) or indirect (I) band gap semi-conductor
[c]Ref. [52]
[d]Mean error
[e]Mean absolute error
[f]Root mean square error
[g]Standard deviation
[h]Maximum negative deviation
[i]Maximum positive deviation

Table 4.7 : Timings for 8 semi-conductors (time for one single point calculation during the geometry optimization, minutes)

Solid	LDA	PBE	TPSS	HSE
C	417	587	1298	2240
Si	411	343	1078	2008
BN	514	757	1460	2817
BP	482	655	1139	1891
SiC	670	774	1584	3477
β-GaN	258	334	625	837
GaP	214	223	417	594
MgO	141	245	505	564
Mean	454	550	1060	2143
Mean (hrs.)	8	9	18	36
Ratio to PBE	0.8	1.0	1.9	3.9

4.4 Timings

In section 2.3.3, we already showed the substantial savings in computational time of HSE over traditional hybrid functionals. Here, we present additional timings for the eight semi-conducting solids. We compare the wall-clock timings for single point calculations using the LDA, PBE, TPSS and HSE functionals.

While the LDA and PBE calculations on average took eight and nine hours, respectively, the meta-GGA TPSS functional was twice as expensive (18 hours) per single point. The HSE screened Coulomb hybrid functional was only twice as computationally expensive as TPSS. Detailed timings can be found in Table 4.7. In practice, once the necessary convergence criteria for a given system are established, the tight

thresholds, used here, can be relaxed. Increasing the thresholds can result in up to a 50% speedup of a given calculation, while still achieving μHartree accuracy.

In light of the superior results exhibited by HSE in the previous sections, the additional CPU time is easily justified. Traditional hybrid functionals such as PBE0 or B3LYP [3] are difficult to converge for these systems and calculations with similarly tight convergence criteria cannot be achieved on commonly available computer hardware.

Chapter 5

Conclusions

For molecules, the HSE screened Coulomb hybrid density functional yields results similar to the established, non-empirical PBE0 hybrid functional on which HSE is based. Enthalpies of formation, optimized geometries and vibrational frequencies are predicted with similar or higher accuracy than that achieved by PBE0. When the common 6-31G* basis set is used for geometry optimizations, both HSE and PBE0 yield significantly better results than the B3LYP functional. For ionization potentials and electron affinities, the three other tested functionals produced smaller errors than HSE. However, the errors produced by HSE are acceptable and might be reduced by enhancing the construction of the functional.

In solids, HSE significantly improves upon GGA and meta-GGA results for structural parameters such as lattice constants and bulk moduli. For non-metallic systems, the error is generally reduced by 50% or more. In metals, HSE still improves upon pure DFT results, but the effect is less dramatic. Band gap calculations of semiconductors, using HSE, produce errors over five times smaller than pure DFT results. Due to the nature of the screened Coulomb interaction approach of HSE, the computational time needed for these calculations is within a factor of two to four of pure DFT calculations. Traditional hybrid calculations need significantly more mem-

ory and CPU time. In addition, the established hybrids exhibit problems with the convergence of the SCF procedure when higher quality basis sets are used.

The comprehensive test results validate our original assumptions in designing HSE. The short range HF exchange exhibits all of the physically relevant properties of the full HF exchange. The same approach used in constructing HSE based on PBE0 can be employed to construct screened Coulomb hybrid functionals based on newer, meta–GGA functionals such as TPSS [4].

The fact that HSE can be applied to metals is extremely useful for applications in molecular electronics and related fields. HSE enables the treatment of molecules attached to conducting surfaces on a hybrid DFT level. Due to the properties of full HF exchange, traditional hybrid functionals cannot be used for such systems.

Overall, the results presented here allow a confident application of the HSE screened Coulomb hybrid functional to both large molecules and solids. The CPU time penalty over pure DFT functionals is more than offset by the superior results provided by this hybrid functional.

Appendix A

FORTRAN reference implementation of the ωPBE short range enhancement factor

```
      Subroutine HSEFx(Rho,s,Omega,FxHSE)
      Implicit Real*8(A-H,O-Z)
C
C     HSE evaluates the Heyd et al. Screened Coulomb
C     Exchange Functional
C
C     Calculates the enhancement factor
C
      Real*8 rho,s,omega,Fxhse
C
      Real*8 A,B,C,D,E
      Real*8 Ha1,Ha2,Ha3,Ha4,Ha5
      Real*8 Fc1,Fc2
      Real*8 ea1,ea2,ea3,ea4,ea5,ea6,ea7,ea8,eb1,wcut
      Real*8 EGscut,EGa1,EGa2,EGa3
      Real*8 expcut,exei1,exei2,exei3,exei4
      Real*8 smax,strans,sconst
C
      Real*8 Zero,One,Two,Three,Four,Five,Six,Seven,Eight,Nine,Ten
      Real*8 FIfteen,Sixteen
      Real*8 r12,r64,r36,r81,r256,r384
      Real*8 r18,r20,r25,r27,r128,r144,r288,r324,r729
      Real*8 r30,r32,r75,r243,r2187,r6561,r40,r105,r54,r135
      Real*8 r1215,r15309
      Real*8 f12,f14,f32,f34,f94,f98,f1516
C
```

```
      Save A,B,C,D,E
      Save Ha1,Ha2,Ha3,Ha4,Ha5
      Save Fc1,Fc2
      Save ea1,ea2,ea3,ea4,ea5,ea6,ea7,ea8,wcut
      Save EGscut,EGa1,EGa2,EGa3
      Save expcut,exei1,exei2,exei3,exei4
      Save smax,strans,sconst
      Save Zero,One,Two,Three,Four,Five,Six,Seven,Eight,Nine,Ten
      Save Fifteen,Sixteen
      Save r36,r64,r81,r256,r384
      Save r27,r128,r144,r288,r324,r729
      Save r18,r20,r32,r243,r2187,r6561,r40
      Save r12,r25,r30,r54,r75,r105,r135,r1215,r15309
      Save f12,f14,f32,f34,f94,f98,f1516
C
C     Constants for PBE hole
C
      Data A,B,C,D,E
     $  / 1.0161144D0,-3.7170836D-1,-7.7215461D-2,
     $    5.7786348D-1,-5.1955731D-2 /
C
C     Constants for fit of H(s) (PBE hole)
C
      Data Ha1,Ha2,Ha3,Ha4,Ha5
     $  / 9.79681d-3,4.10834d-2,1.87440d-1,1.20824d-3,3.47188d-2 /
C
C     Constants for F(H) (PBE hole)
C
      Data Fc1,Fc2 / 6.4753871d0,4.7965830d-1 /
C
C     Constants for expansion of erfc(x) (eb1 set later
```

```
C     depending on wcut)
C
      Data ea1,ea2,ea3,ea4,ea5,ea6,ea7,ea8,wcut
     $  / -1.128223946706117d0,1.452736265762971d0,
     $    -1.243162299390327d0,0.971824836115601d0,
     $    -0.568861079687373d0,0.246880514820192d0,
     $    -0.065032363850763d0,0.008401793031216d0,1.4D1 /
C
C     Constants for polynomial expansion of EG for small s
C
      Data EGscut,EGa1,EGa2,EGa3
     $  / 8.0d-2,-2.628417880d-2,-7.117647788d-2,8.534541323d-2 /
C
C     Constants for large x expansion of exp(x)*ei(-x)
C
      Data expcut,exei1,exei2,exei3,exei4
     $  / 7.0D2,4.03640D0,1.15198D0,5.03627D0,4.19160D0 /
C
C     Constants for enforcement of local Lieb-Oxford bound
C
      Data smax,strans,sconst
     $  / 8.572844D0,8.3D0,1.879622316D1 /
C
C     Whole numbers used during evaluation
C
      Data Zero,One,Two,Three,Four,Five,Six,Seven,Eight,Nine,Ten
     $  / 0D0,1D0,2D0,3D0,4D0,5D0,6D0,7D0,8D0,9D0,10D0 /
      Data FIfteen,Sixteen / 1.5D1, 1.6D1 /
      Data r36,r64,r81,r256,r384
     $  / 3.6D1,6.4D1,8.1D1,2.56D2,3.84D2 /
      Data r27,r128,r144,r288,r324,r729
```

```
     $  / 2.7D1,1.28D2,1.44D2,2.88D2,3.24D2,7.29D2 /
      Data r18,r20,r32,r243,r2187,r6561,r40
     $  / 1.8d1,2.0d1,3.2D1,2.43D2,2.187D3,6.561D3,4.0d1 /
      Data r12,r25,r30,r54,r75,r105,r135,r1215,r15309
     $  / 1.2D1,2.5d1,3.0d1,5.4D1,7.5d1,1.05D2,1.35D2,1.215D3,
     $    1.5309D4 /
C
C     Fractions used during evaluation
C
      Data f12,f14,f32,f34,f94,f98,f1516
     $  / 0.5D0,0.25D0,1.5D0,0.75D0,2.25D0,1.125D0,0.9375D0 /
C
C     General constants
C
      f13  = One/Three
      pi   = ACos(-One)
      pi2  = pi*pi
      srpi = sqrt(pi)
      X    = -Eight/Nine
C
C     Cutoff criterion to enforce local Lieb-Oxford bound
C     This ensures that the enhancement factor does not exceed the
C     one of the original PBE functional (Fx(max)=1.804).
C
      sreal       = s
      If(s.gt.strans) then
        s = smax-(sconst/sreal**2)
        stra1s = Two*sconst/sreal**3
      else
        stra1s = One
      endIf
```

```
C
C     Calculate prelim variables
C
      xkf    = (Three*pi2*rho) ** f13
      A2   = A*A
      A3   = A2*A
      A4   = A3*A
      A12  = Sqrt(A)
      A32  = A12*A
      A52  = A32*A
      w    = omega / xkf
      w2   = w * w
      w3   = w2 * w
      w4   = w2 * w2
      w5   = w3 * w2
      w6   = w5 * w
      w7   = w6 * w
      w8   = w7 * w
      s2   = s*s
      s3   = s2*s
      s4   = s2*s2
      s5   = s4*s
      s6   = s5*s
C
C     Calculate H(s) and F(H(s)) for the PBE hole
C
      Hnum  = Ha1*s2 + Ha2*s4
      Hden  = One + Ha3*s4 + Ha4*s5 + Ha5*s6
      H     = Hnum/Hden
      Hnu1s = Two*Ha1*s + Four*Ha2*s3
      Hde1s = Four*Ha3*s3 + Five*Ha4*s4 + Six*Ha5*s5
```

```
      H1s   = (Hden*Hnu1s - Hnum*Hde1s) / (Hden*Hden)
      F     = Fc1*H + Fc2
C
C     Set exponent of Gaussian in approx depending on which approx
C     we use for erfc(x)
C
      If(w .lt. wcut) then
        eb1 = 1.455915450052607d0
      else
        eb1 = 2.0d0
      endIf
C
C     Calculate helper variables
C
      Hsbw   = s2*H + eb1*w2
      Hsbw2  = Hsbw*Hsbw
      Hsbw3  = Hsbw2*Hsbw
      Hsbw4  = Hsbw3*Hsbw
      Hsbw6  = Hsbw3*Hsbw3
      Hsbw12 = Sqrt(Hsbw)
      Hsbw32 = Hsbw12*Hsbw
      Hsbw52 = Hsbw32*Hsbw
      Hsbw72 = Hsbw52*Hsbw
      DHsb   = D + s2*H + eb1*w2
      DHsb2  = DHsb*DHsb
      DHsb3  = DHsb2*DHsb
      DHsb4  = DHsb3*DHsb
      DHsb5  = DHsb4*DHsb
      DHsb12 = Sqrt(DHsb)
      DHsb32 = DHsb12*DHsb
      DHsb52 = DHsb32*DHsb
```

```
      DHsb72 = DHsb52*DHsb
      DHsb92 = DHsb72*DHsb
      HA94   = f94 * Hsbw / A
      HA942  = HA94*HA94
      HA943  = HA942*HA94
      HA945  = HA943*HA942
      HA9412 = Sqrt(HA94)
      DHs    = D + s2*H
      DHs2   = DHs*DHs
      DHs3   = DHs2*DHs
      DHs4   = DHs3*DHs
      DHs72  = DHs3*sqrt(DHs)
      DHs92  = DHs72*DHs
      DHsw   = DHs + w2
      DHsw2  = DHsw*DHsw
      DHsw52 = sqrt(DHsw)*DHsw2
      DHsw72 = DHsw52*DHsw
C
C     Calculate EG(s), using expansion for small s If necessary
C
      If(s .gt. EGscut) then
        G_a  = srpi * (FIfteen*E + Six*C*(One+F*s2)*DHs +
     $                 Four*B*(DHs2) + Eight*A*(DHs3))
     $              * (One / (Sixteen * DHs72))
     $              - f34*pi*sqrt(A) * GExp(f94*H*s2/A) *
     $                (One - gerf(f32*s*sqrt(H/A)))
        G_b  = (f1516 * srpi * s2) / DHs72
        EG   = - (f34*pi + G_a) / G_b
      else
        EG   = EGa1 + EGa2*s2 + EGa3*s4
      endIf
```

```
C
C    Calculate the terms needed in any case
C
      tm2    = (DHs2*B + DHs*C + Two*E + DHs*s2*C*F + Two*s2*EG) /
     $         (Two*DHs3)
      tm3    = - w  * (Four*DHsw2*B + Six*DHsw*C + FIfteen*E
     $                + Six*DHsw*s2*C*F + FIfteen*s2*EG) /
     $                (Eight*DHs*DHsw52)
      tm4    = - w3 * (DHsw*C + Five*E + DHsw*s2*C*F + Five*s2*EG) /
     $                (Two*DHs2*DHsw52)
      tm5    = - w5 * (E + s2*EG) / (DHs3*DHsw52)
C
C     Calculate t10 unless that would generate a div. by zero
C
      If((s.gt.0.0d0).or.(w.gt.0.0d0)) then
        t10    = (f12)*A*Log(Hsbw / DHsb)
      endIf
C
C     Calculate exp(x)*f(x) depending on size of x
C
      If(HA94 .lt. expcut) then
        exer   = pi*GExp(HA94)*GErfc(HA9412)
        exHA94 = GExp(HA94)
        eiHA94 = GEi(-HA94)
        exei   = exHA94*eiHA94
      else
        exer   = pi*(One/(srpi*HA9412)
     $              - One/(Two*Sqrt(pi*HA943))
     $              + Three/(Four*Sqrt(pi*HA945)))
        exei   = - (One/HA94) *
     $             (HA942 + exei1*HA94 + exei2) /
```

```
     $             (HA942 + exei3*HA94 + exei4)
      endIf
C
      If (w .eq. Zero) then
C
C       Fall back to original expression for the PBE hole
C
        t1    = -f12*A*exei
C
        If(s .gt. 0.0D0) then
          tm1    = t1 + t10

          Fxhse  = X * (tm1 + tm2)

        else
          Fxhse  = 1.0d0
        endIf
C
      else If(w .gt. wcut) then
C
C       Use simple Gaussian approximation for large w
C
        tm1    = -f12*A*(exei+log(DHsb)-log(Hsbw))
        Fxhse  = X * (tm1 + tm2 + tm3 + tm4 + tm5)
      else
C
C       For everything else, use the full blown expression
C
C       First, we calculate the polynomials for the first term
C
        pn1    = -f32*ea1*A12*w + r27*ea3*w3/(Eight*A12)
```

```
     $           - r243*ea5*w5/(r32*A32) + r2187*ea7*w7/(r128*A52)
        pn2    = -A + f94*ea2*w2 - r81*ea4*w4/(Sixteen*A)
     $           + r729*ea6*w6/(r64*A2) - r6561*ea8*w8/(r256*A3)
C
C       The first term is
C
        t1    = f12*(pn1*exer + pn2*exei)
C
C       The factors for the main polynomoal in w
C
        f2     = (f12)*ea1*srpi*A / DHsb12
        f3     = (f12)*ea2*A / DHsb
        f4     =  ea3*srpi*(-f98 / Hsbw12
     $            + f14*A / DHsb32)
        f5     = ea4*(One/r128) * (-r144*(One/Hsbw)
     $            + r64*(One/DHsb2)*A)
        f6     = ea5*(Three*srpi*(Three*DHsb52*(Nine*Hsbw-Two*A)
     $           + Four*Hsbw32*A2))
     $           / (r32*DHsb52*Hsbw32*A)
        f7     = ea6*(((r32*A)/DHsb3
     $            + (-r36 + (r81*s2*H)/A)/Hsbw2)) / r32
        f8     = ea7*(-Three*srpi*(-r40*Hsbw52*A3
     $            +Nine*DHsb72*(r27*Hsbw2-Six*Hsbw*A+Four*A2)))
     $            / (r128 * DHsb72*Hsbw52*A2)
        f9     = (r324*ea6*eb1*DHsb4*Hsbw*A
     $           + ea8*(r384*Hsbw3*A3 + DHsb4*(-r729*Hsbw2
     $           + r324*Hsbw*A - r288*A2))) / (r128*DHsb4*Hsbw3*A2)
C
        t2t9   = f2*w  + f3*w2 + f4*w3 + f5*w4 + f6*w5
     $           + f7*w6 + f8*w7 + f9*w8
C
```

```
C       The final value of term1 for 0 < omega < wcut is:
C
        tm1    = t1 + t2t9 + t10
C
C       The final value for the enhancement factor is
C
        Fxhse = X * (tm1 + tm2 + tm3 + tm4 + tm5)

      endIf
C
      end
```

Appendix B

Computational details

The HSE functional and its analytical first derivatives was implemented into the *Gaussian* suite of programs[16]. The following sections give additional details about the calculations whose results are presented in the main chapters.

B.1 Calculations on atoms and molecules

The 6-311++G(3df,3pd) basis set was used in self-consistent, spin unrestricted Kohn-Sham calculations of atomic energies, enthalpies of formation, geometry optimizations, vibrational frequencies, and ionization potentials, as well as electron affinities. This basis, when used in hybrid DFT calculations, provides a model chemistry which gives results close to the basis set limit. In addition, geometry optimizations and vibrational frequency calculations were also carried out using the 6-31G* basis set which is commonly used for these types of calculations.

The enthalpies of formation were calculated both using geometries optimized at the MP2/6-31G* level and then using geometries optimized with each functional and the 6-311++G(3df,3pd) basis set. Standard enthalpies of formation were obtained by the procedure described in Ref. [36]. For both the zero point energy and the thermal enthalpy corrections, HF/6-31G* frequencies scaled with a factor of $f = 0.8929$ were

used.

Geometry optimizations employed analytical gradients while harmonic vibrational frequencies were calculated via numerical differentiation of analytic first derivatives (for HSE only, all other functionals used analytic second derivatives).

The transition metal hexacarbonyl geometry optimizations used a Stuttgart 97 small core relativistic effective core potential (ECP) on the metal and 6-311G(d) basis sets on carbon and oxygen. The partial charges were determined by natural bond orbital (NBO) analysis [57] using the same ECP on the metal and the 6-311G(2df) basis set on carbon and oxygen.

B.2 Calculations on solids

All calculations employed the periodic boundary condition (PBC) code[34] available in *Gaussian*. Three-dimensional, self-consistent, spin-restricted Kohn-Sham calculations were performed on all systems. The short range HF exchange interactions were calculated in real space using an adaptation of the NFX method[35] for periodic systems. Gaussian basis sets were used throughout this work. We employed a standard molecular basis whenever possible. For some solids, however, other optimized basis sets from the literature were used. Table 4.1 lists the detailed basis sets used for each system.

All calculations converged the SCF procedure to an accuracy of 10^{-8}. Only SR exchange integrals smaller than 10^{-12} were neglected. The reciprocal space integration

was performed using 24 k-points in each dimension for a total of 6912 k-points. In practice, these thresholds can be relaxed after a preliminary study of a given system. The goal of the present work, however, is to establish the accuracy of the various DFT methods examined. Therefore, we only show fully converged results.

Lattice constants and bulk moduli were determined using the Murnaghan equation of state[53] (EOS). The experimental equilibrium lattice constant was perturbed in steps of 0.05 Å and a total of nine calculations was performed. To obtain the band gaps, single point calculations were performed at the optimized lattice constants (for each method). Unless otherwise noted, experimental results were taken from Ref. [6].

All calculations were carried out on dual processor AMD AthlonXP2100+ systems with 2 GB of memory. The silicon calculations demonstrating screening efficiency and convergence used one CPU, all other calculations were run in parallel on two CPUs. Wall-clock times are used throughout.

Appendix C

Detailed results for molecules

This appendix contains the detailed results of all molecular calculations with the HSE hybrid functional. Presented are enthalpies of formation, bond length optimizations, ionization potentials, and electron affinities.

Table C.1 : HSE/6-311++G(3df,3pd) standard enthalpies of formation at 298K for the G3 set (kcal/mol)

Molecule	ΣD_e [a]	ZPE [b]	ΣD_0 [c]	$\Delta_f H^\circ_{0K}$	$\Delta_f H^\circ_{298K}$	$\Delta_f H^\circ_{298K}$(exp.)[d]	Dev.[e]
G2-1 test set							
LiH	54.0	1.8	52.2	37.1	37.1	33.3	3.8
BeH	57.0	2.7	54.3	73.8	74.4	81.7	−7.3
CH	83.3	3.9	79.4	142.3	143.1	142.5	0.6
CH_2 ($^3B_1$)	194.0	10.3	183.6	89.6	89.7	93.7	−4.0
CH_2 ($^1A_1$)	176.7	10.1	166.6	106.7	106.8	102.8	4.0
CH_3	308.8	17.4	291.4	33.5	32.9	35.0	−2.1
CH_4	417.9	26.8	391.1	−14.6	−16.5	−17.9	1.4
NH	85.6	4.5	81.1	83.1	83.1	85.2	−2.1
NH_2	183.5	11.5	171.9	43.8	43.2	45.1	−1.9
NH_3	295.2	20.7	274.4	−7.0	−8.7	−11.0	2.3
OH	106.0	5.1	100.9	9.7	9.7	9.4	0.3
H_2O	227.4	12.9	214.5	−52.2	−52.9	−57.8	4.9
FH	137.3	5.6	131.7	−61.6	−61.6	−65.1	3.5
SiH_2 ($^1A_1$)	147.6	7.1	140.5	69.4	69.0	65.2	3.8
SiH_2 ($^3B_1$)	132.4	7.3	125.1	84.8	84.4	86.2	−1.8
SiH_3	224.0	12.8	211.2	50.3	49.0	47.9	1.1
SiH_4	316.0	18.8	297.3	15.8	13.6	8.2	5.4
PH_2	153.8	8.2	145.6	33.0	32.1	33.1	−1.0

Table C.1 : HSE/6-311++G(3df,3pd) standard enthalpies of formation at 298K for the G3 set (kcal/mol)

Molecule	ΣD_e [a]	ZPE [b]	ΣD_0 [c]	$\Delta_f H^\circ_{0K}$	$\Delta_f H^\circ_{298K}$	$\Delta_f H^\circ_{298K}$(exp.)[d]	Dev.[e]
PH_3	238.3	14.7	223.6	6.7	4.8	1.3	3.5
H_2S	180.1	9.2	170.9	−1.9	−2.6	−4.9	2.3
HCl	105.4	4.1	101.3	−21.1	−21.1	−22.1	1.0
Li_2	19.5	0.4	19.1	56.3	56.4	51.6	4.8
LiF	134.8	1.3	133.5	−77.3	−77.3	−80.1	2.8
HC≡CH	403.9	16.5	387.4	55.8	55.6	54.2	1.4
CH_2=CH_2	563.9	30.7	533.2	13.3	11.2	12.5	−1.3
CH_3CH_3	712.2	44.7	667.5	−17.8	−21.5	−20.1	−1.4
CN	178.2	2.5	175.7	106.8	107.6	104.9	2.7
HCN	310.2	10.1	300.1	34.0	33.9	31.5	2.4
CO	254.9	3.1	251.7	−22.8	−22.0	−26.4	4.4
CHO	280.7	8.1	272.6	8.0	8.1	10.0	−1.9
CH_2O	372.7	16.4	356.4	−24.1	−25.1	−26.0	0.9
CH_3OH	510.5	31.0	479.5	−44.0	−46.7	−48.0	1.3
N_2	222.3	3.5	218.8	6.3	6.2	0.0	6.2
N_2H_4	438.2	32.5	405.6	25.9	22.5	22.8	−0.3
NO	153.5	2.8	150.6	20.9	20.9	21.6	−0.7
O_2	121.1	2.6	118.5	−0.5	−0.5	0.0	−0.5
H_2O_2	262.5	16.4	246.1	−24.9	−26.4	−32.5	6.1

Table C.1 : HSE/6-311++G(3df,3pd) standard enthalpies of formation at 298K for the G3 set (kcal/mol)

Molecule	ΣD_e [a]	ZPE [b]	ΣD_0 [c]	$\Delta_f H^\circ_{0K}$	$\Delta_f H^\circ_{298K}$	$\Delta_f H^\circ_{298K}$(exp.)[d]	Dev.[e]
F_2	32.9	1.6	31.3	5.7	5.7	0.0	5.7
CO_2	391.7	7.1	384.6	−96.6	−96.7	−94.1	−2.6
Na_2	16.1	0.2	15.9	35.4	34.8	34.0	0.8
Si_2	77.1	0.7	76.4	136.8	137.5	139.9	−2.4
P_2	111.1	1.2	109.9	40.9	40.5	34.3	6.2
S_2	105.8	1.0	104.8	26.5	26.6	30.7	−4.1
Cl_2	58.5	0.8	57.8	−0.6	−0.6	0.0	−0.6
NaCl	96.1	0.5	95.7	−41.4	−41.7	−43.6	1.9
SiO	182.0	1.8	180.2	−14.6	−14.3	−24.6	10.3
CS	167.7	1.8	165.8	69.8	70.6	66.9	3.7
SO	125.1	1.7	123.4	1.3	1.3	1.2	0.1
ClO	66.2	1.1	65.1	22.5	22.5	24.2	−1.7
ClF	60.2	1.2	59.1	−12.0	−12.0	−13.2	1.2
Si_2H_6	523.6	29.5	494.1	28.9	25.1	19.1	6.0
CH_3Cl	396.0	22.8	373.2	−19.7	−21.6	−19.6	−2.0
CH_3SH	473.2	27.8	445.4	−3.3	−5.7	−5.5	−0.2
HOCl	162.3	8.1	154.2	−15.0	−15.7	−17.8	2.1
SO_2	248.2	4.5	243.7	−60.0	−60.7	−71.0	10.3
G2-2 test set							

Table C.1 : HSE/6-311++G(3df,3pd) standard enthalpies of formation at 298K for the G3 set (kcal/mol)

Molecule	ΣD_e [a]	ZPE [b]	ΣD_0 [c]	$\Delta_f H^\circ_{0K}$	$\Delta_f H^\circ_{298K}$	$\Delta_f H^\circ_{298K}$(exp.)[d]	Dev.[e]
Non-hydrogen systems							
BF_3	468.6	7.5	461.1	−269.5	−270.1	−271.4	1.3
BCl_3	331.7	4.5	327.1	−105.1	−105.3	−96.3	−9.0
AlF_3	413.9	4.7	409.2	−275.6	−276.4	−289.0	12.6
$AlCl_3$	307.9	2.8	305.1	−141.1	−141.4	−139.7	−1.7
CF_4	480.5	10.7	469.8	−225.9	−227.3	−223.0	−4.3
CCl_4	320.0	6.1	314.0	−29.6	−30.2	−22.9	−7.3
COS	338.2	5.5	332.7	−38.1	−38.0	−33.1	−4.9
CS_2	283.9	4.1	279.8	21.5	21.7	28.0	−6.3
COF_2	423.1	8.8	414.2	−148.3	−149.0	−149.1	0.1
SiF_4	552.9	7.6	545.3	−364.8	−366.0	−386.0	20.0
$SiCl_4$	383.1	4.4	378.7	−157.7	−158.2	−158.4	0.2
N_2O	271.7	6.9	264.8	19.2	18.4	19.6	−1.2
NOCl	191.5	4.0	187.5	12.6	12.1	12.4	−0.3
NF_3	209.0	7.1	201.9	−33.9	−35.4	−31.6	−3.8
PF_3	354.1	5.3	348.9	−218.0	−219.3	−229.1	9.8
O_3	134.3	4.9	129.4	47.6	46.9	34.1	12.8
F_2O	89.1	3.8	85.3	10.6	10.0	5.9	4.1
ClF_3	128.4	4.7	123.7	−39.7	−40.7	−38.0	−2.7

Table C.1 : HSE/6-311++G(3df,3pd) standard enthalpies of formation at 298K for the G3 set (kcal/mol)

Molecule	ΣD_e [a]	ZPE [b]	ΣD_0 [c]	$\Delta_f H^\circ_{0K}$	$\Delta_f H^\circ_{298K}$	$\Delta_f H^\circ_{298K}$(exp.)[d]	Dev.[e]
CF_2=CF_2	598.5	13.4	585.1	−171.2	−172.0	−157.4	−14.6
CCl_2=CCl_2	481.8	9.6	472.1	−17.8	−18.0	−3.0	−15.0
CF_3CN	645.1	14.3	630.8	−122.9	−123.8	−118.4	−5.4
Hydrocarbons							
$CH_3C{\equiv}CH$ (propyne)	707.4	33.7	673.7	42.7	41.0	44.2	−3.2
CH_2=C=CH_2 (allene)	709.4	33.3	676.1	40.4	38.6	45.5	−6.9
C_3H_4 (cyclopropene)	688.6	33.9	654.7	61.8	59.7	66.2	−6.5
CH_3CH=CH_2 (propylene)	863.3	47.9	815.5	4.3	0.7	4.8	−4.1
C_3H_6 (cyclopropane)	859.5	48.9	810.6	9.1	5.0	12.7	−7.7
C_3H_8 (propane)	1008.0	62.0	946.1	−23.1	−28.4	−25.0	−3.4
C_4H_6 (1,3-butadiene)	1018.2	51.3	966.9	22.8	19.3	26.3	−7.0
C_4H_6 (2-butyne)	1009.6	50.8	958.8	30.9	28.0	34.8	−6.8
C_4H_6 (methylene cyclopropane)	1003.0	51.4	951.6	38.1	34.3	47.9	−13.6
C_4H_6 (bicyclobutane)	997.7	52.2	945.6	44.1	40.0	51.9	−11.9
C_4H_6 (cyclobutene)	1009.0	52.2	956.8	32.9	28.9	37.4	−8.5
C_4H_8 (cyclobutane)	1156.1	66.6	1089.5	3.5	−2.4	6.8	−9.2
C_4H_8 (isobutene)	1162.6	64.8	1097.8	−4.9	−9.9	−4.0	−5.9
C_4H_{10} (butane)	1303.8	79.1	1224.7	−28.5	−35.3	−30.0	−5.3
C_4H_{10} (isobutane)	1304.6	78.9	1225.8	−29.5	−36.4	−32.1	−4.3

Table C.1 : HSE/6-311++G(3df,3pd) standard enthalpies of formation at 298K for the G3 set (kcal/mol)

Molecule	ΣD_e [a]	ZPE [b]	ΣD_0 [c]	$\Delta_f H^\circ_{0K}$	$\Delta_f H^\circ_{298K}$	$\Delta_f H^\circ_{298K}$(exp.)[d]	Dev.[e]
C_5H_8 (spiropentane)	1299.4	69.3	1230.1	32.9	27.3	44.3	−17.0
C_6H_6 (benzene)	1385.0	60.3	1324.7	4.9	0.8	19.7	−18.9
Substituted hydrocarbons							
CH_2F_2	438.0	20.2	417.8	−107.6	−109.4	−107.7	−1.7
CHF_3	460.6	15.8	444.8	−167.8	−169.4	−166.6	−2.8
CH_2Cl_2	373.8	18.0	355.9	−25.5	−27.1	−22.8	−4.3
$CHCl_3$	349.2	12.3	336.8	−29.4	−30.6	−24.7	−5.9
CH_3NH_2 (methylamine)	581.7	38.6	543.1	−2.4	−6.0	−5.5	−0.5
CH_3CN (acetonitrile)	617.2	27.4	589.8	17.6	15.9	18.0	−2.1
CH_3NO_2 (nitromethane)	604.8	30.6	574.3	−18.9	−21.9	−17.8	−4.1
CH_3ONO (methyl nitrite)	599.6	30.1	569.5	−14.1	−17.2	−15.9	−1.3
CH_3SiH_3 (methyl silane)	621.7	36.5	585.2	1.1	−2.6	−7.0	4.4
HCOOH (formic acid)	501.2	20.8	480.4	−89.2	−91.0	−90.5	−0.5
$HCOOCH_3$ (methyl formate)	787.6	37.9	749.7	−85.3	−88.4	−85.0	−3.4
CH_3CONH_2 (acetamide)	872.7	44.3	828.4	−58.8	−62.5	−57.0	−5.5
C_2H_4NH (aziridine)	725.9	42.6	683.4	27.3	23.3	30.2	−6.9
$(CN)_2$ (cyanogen)	503.2	10.2	493.0	72.0	72.4	73.3	−0.9
$(CH_3)_2NH$ (dimethylamine)	871.6	55.7	815.8	−1.9	−7.1	−4.4	−2.7
$CH_3CH_2NH_2$ (ethylamine)	879.3	55.8	823.5	−9.6	−14.9	−11.3	−3.6

Table C.1 : HSE/6-311++G(3df,3pd) standard enthalpies of formation at 298K for the G3 set (kcal/mol)

Molecule	ΣD_e [a]	ZPE [b]	ΣD_0 [c]	$\Delta_f H^\circ_{0K}$	$\Delta_f H^\circ_{298K}$	$\Delta_f H^\circ_{298K}$(exp.)[d]	Dev.[e]
CH_2=C=O (ketene)	538.2	19.2	519.0	−16.8	−17.6	−11.4	−6.2
C_2H_4O (oxirane)	654.6	34.9	619.7	−14.2	−17.2	−12.6	−4.6
CH_3CHO (acetaldehyde)	678.6	33.6	645.0	−39.6	−42.1	−39.7	−2.4
HCOCHO (glyoxal)	635.7	22.9	612.8	−51.6	−53.0	−50.7	−2.3
CH_3CH_2OH (ethanol)	809.5	48.2	761.3	−52.5	−56.8	−56.2	−0.6
CH_3OCH_3 (dimethyl ether)	797.7	48.3	749.4	−40.7	−44.9	−44.0	−0.9
C_2H_4S (thiirane)	629.8	33.3	596.5	15.6	12.8	19.6	−6.8
$(CH_3)_2SO$ (dimethyl sulfoxide)	854.2	48.1	806.1	−31.7	−36.3	−36.2	−0.1
C_2H_5SH (ethanethiol)	769.5	45.1	724.4	−9.0	−13.0	−11.1	−1.9
CH_3SCH_3 (dimethyl sulfide)	768.5	45.7	722.8	−7.4	−11.4	−8.9	−2.5
CH_2=CHF (vinyl fluoride)	576.1	26.7	549.4	−36.1	−38.0	−33.2	−4.8
C_2H_5Cl (ethyl chloride)	694.2	40.1	654.1	−27.4	−30.9	−26.8	−4.1
CH_2=CHCl (vinyl chloride)	547.2	25.9	521.3	2.1	0.3	8.9	−8.6
CH_2=CHCN (acrylonitrile)	766.3	30.8	735.6	41.8	40.2	43.2	−3.0
CH_3COCH_3 (acetone)	982.0	50.4	931.6	−52.9	−56.7	−51.9	−4.8
CH_3COOH (acetic acid)	805.0	37.5	767.5	−103.1	−106.2	−103.4	−2.8
CH_3COF (acetyl fluoride)	709.6	29.7	679.8	−107.5	−109.8	−105.7	−4.1
CH_3COCl (acetyl chloride)	673.0	28.6	644.4	−62.0	−64.1	−58.0	−6.1
$CH_3CH_2CH_2Cl$ (propyl chloride)	990.0	57.2	932.8	−32.8	−37.8	−31.5	−6.3

Table C.1 : HSE/6-311++G(3df,3pd) standard enthalpies of formation at 298K for the G3 set (kcal/mol)

Molecule	ΣD_e [a]	ZPE [b]	ΣD_0 [c]	$\Delta_f H^\circ_{0K}$	$\Delta_f H^\circ_{298K}$	$\Delta_f H^\circ_{298K}$(exp.)[d]	Dev.[e]
$(CH_3)_2CHOH$ (isopropanol)	1108.5	65.0	1043.5	−61.5	−67.3	−65.2	−2.1
$C_2H_5OCH_3$ (methyl ethyl ether)	1096.6	65.3	1031.3	−49.3	−55.1	−51.7	−3.4
$(CH_3)_3N$ (trimethylamine)	1163.3	72.6	1090.7	−3.6	−10.4	−5.7	−4.7
C_4H_4O (furan)	1005.4	42.4	962.9	−17.5	−20.7	−8.3	−12.4
C_4H_4S (thiophene)	975.0	40.4	934.6	17.5	14.6	27.5	−12.9
C_4H_5N (pyrrole)	1086.2	49.7	1036.5	14.1	10.2	25.9	−15.7
C_5H_5N (pyridine)	1255.7	53.5	1202.3	18.3	14.3	33.6	−19.3
Inorganic hydrides							
H_2	104.5	5.9	98.5	4.7	4.8	0.0	4.8
SH	87.0	3.7	83.2	34.0	34.1	34.2	−0.1
Radicals							
C≡CH	266.3	8.4	257.9	133.7	134.6	135.1	−0.5
CH=CH_2 ($^2A'$)	449.9	21.7	428.2	66.6	65.7	71.6	−5.9
CH_3CO ($^2A'$)	586.4	26.1	560.4	−6.5	−8.0	−2.4	−5.6
CH_2OH (^2A)	411.3	22.5	388.8	−4.9	−6.6	−4.1	−2.5
CH_3O ($^2A'$)	403.6	22.6	381.0	2.8	1.0	4.1	−3.1
CH_3CH_2O ($^2A''$)	699.2	39.3	659.9	−2.8	−6.1	−3.7	−2.4
CH_3S ($^2A'$)	384.4	21.6	362.9	27.7	26.0	29.8	−3.8
CH_3CH_2 ($^2A'$)	607.6	35.5	572.1	26.0	23.6	28.9	−5.3

Table C.1 : HSE/6-311++G(3df,3pd) standard enthalpies of formation at 298K for the G3 set (kcal/mol)

Molecule	ΣD_e [a]	ZPE [b]	ΣD_0 [c]	$\Delta_f H^\circ_{0K}$	$\Delta_f H^\circ_{298K}$	$\Delta_f H^\circ_{298K}$(exp.)[d]	Dev.[e]
$(CH_3)_2CH$ ($^2A'$)	907.0	53.0	854.0	17.3	13.3	21.5	−8.2
$(CH_3)_3C$ (*t*-butyl radical)	1206.5	70.2	1136.3	8.3	2.8	12.3	−9.5
NO_2	231.9	5.5	226.4	4.1	3.4	7.9	−4.5
G3 test set							
CH_2=C=$CHCH_3$	1007.4	50.6	956.8	32.9	29.6	38.8	−9.2
CH_2=CH–$C(CH_3)$=CH_2	1316.8	68.3	1248.5	14.5	9.5	18.0	−8.5
C_5H_{10} (cyclopentane)	1471.3	84.4	1386.8	−20.6	−28.0	−18.3	−9.7
C_5H_{12} (*n*-pentane)	1599.5	96.2	1503.3	−33.8	−42.0	−35.1	−6.9
$C(CH_3)_4$ (neopentane)	1601.2	95.6	1505.6	−36.1	−44.5	−40.2	−4.3
C_6H_8 (1,3-cyclohexadiene)	1489.6	73.8	1415.8	17.1	11.5	25.4	−13.9
C_6H_8 (1,4-cyclohexadiene)	1489.8	73.7	1416.1	16.8	11.2	25.0	−13.8
C_6H_{12} (cyclohexane)	1772.8	102.2	1670.6	−31.2	−40.5	−29.5	−11.0
C_6H_{14} (*n*-hexane)	1895.2	113.3	1781.9	−39.2	−48.8	−39.9	−8.9
C_6H_{14} (3-methyl pentane)	1894.4	113.2	1781.2	−38.5	−48.1	−41.1	−7.0
$C_6H_5CH_3$ (toluene)	1683.1	76.7	1606.4	−3.5	−8.7	12.0	−20.7
C_7H_{16} (*n*-heptane)	2190.9	130.4	2060.5	−44.5	−55.6	−44.9	−10.7
C_8H_8 (cyclooctatetraene)	1796.1	80.3	1715.8	57.1	51.9	70.7	−18.8
C_8H_{18} (*n*-octane)	2486.6	147.5	2339.1	−49.9	−62.3	−49.9	−12.4
$C_{10}H_8$ (naphthalene)	2195.0	88.6	2106.3	6.5	0.9	35.9	−35.0

Table C.1 : HSE/6-311++G(3df,3pd) standard enthalpies of formation at 298K for the G3 set (kcal/mol)

Molecule	ΣD_e [a]	ZPE [b]	ΣD_0 [c]	$\Delta_f H^\circ_{0K}$	$\Delta_f H^\circ_{298K}$	$\Delta_f H^\circ_{298K}$(exp.)[d]	Dev.[e]
$C_{10}H_8$ (azulene)	2160.4	86.6	2073.8	39.1	33.6	69.1	−35.5
CH_3COOCH_3	1090.8	54.4	1036.4	−98.7	−103.1	−98.4	−4.7
$(CH_3)_3COH$ (*t*-butanol)	1406.7	81.6	1325.1	−69.9	−77.1	−74.7	−2.4
$C_6H_5NH_2$ (aniline)	1560.2	70.4	1489.8	4.0	−1.3	20.8	−22.1
C_6H_5OH (phenol)	1489.1	62.9	1426.2	−37.5	−41.9	−23.0	−18.9
CH_2=CH–O–CH=CH_2	1110.0	53.8	1056.2	−7.5	−11.2	−3.3	−7.9
C_4H_8O (tetrahydrofuran)	1267.7	70.6	1197.2	−45.2	−51.6	−44.0	−7.6
C_5H_8O (cyclopentanone)	1447.6	73.1	1374.4	−52.5	−58.7	−45.9	−12.8
$C_6H_4O_2$ (1,4-benzoquinone)	1438.6	51.8	1386.8	−42.4	−45.5	−29.4	−16.1
$C_4H_4N_2$ (pyrimidine)	1128.4	46.7	1081.7	29.8	25.9	46.8	−20.9
$(CH_3)_2SO_2$	965.7	51.7	914.0	−80.6	−85.8	−89.2	3.4
C_6H_5Cl (chlorobenzene)	1367.5	54.8	1312.7	−6.1	−9.6	12.4	−22.0
NC–CH_2CH_2–CN	1109.1	44.6	1064.5	47.0	44.4	50.1	−5.7
$C_4H_4N_2$ (pyrazine)	1123.8	46.5	1077.4	34.1	30.3	46.9	−16.6
$CH_3COC{\equiv}CH$	971.2	39.7	931.5	13.9	11.9	15.6	−3.7
CH_3–CH=CH–CHO	1132.3	54.1	1078.2	−29.5	−33.3	−24.0	−9.3
$(CH_3CO)_2O$	1367.9	59.6	1308.3	−141.6	−146.1	−136.8	−9.3
C_4H_6S (2,5-dihydrothiophene)	1095.1	54.2	1040.8	14.5	10.1	20.8	−10.7
CH_3–$CH(CH_3)$–CN	1208.9	61.7	1147.2	6.7	2.0	5.6	−3.6

Table C.1 : HSE/6-311++G(3df,3pd) standard enthalpies of formation at 298K for the G3 set (kcal/mol)

Molecule	ΣD_e [a]	ZPE [b]	ΣD_0 [c]	$\Delta_f H^\circ_{0K}$	$\Delta_f H^\circ_{298K}$	$\Delta_f H^\circ_{298K}$(exp.)[d]	Dev.[e]
CH_3–CO–CH_2CH_3	1278.0	67.7	1210.3	−58.4	−63.7	−57.1	−6.6
$(CH_3)_2$CH–CHO	1270.4	67.9	1202.5	−50.6	−56.0	−51.6	−4.4
$C_4H_8O_2$ (1,4-dioxane)	1360.8	74.4	1286.4	−75.5	−82.7	−75.5	−7.2
C_4H_8S (tetrahydrothiophene)	1237.6	68.7	1169.0	−10.3	−16.6	−8.2	−8.4
$(CH_3)_3$C–Cl	1290.1	73.6	1216.5	−43.3	−49.7	−43.5	−6.2
$CH_3CH_2CH_2CH_2Cl$	1285.6	74.4	1211.2	−38.0	−44.3	−37.0	−7.3
C_4H_8NH (pyrrolidine)	1338.6	78.2	1260.4	−3.3	−10.7	−0.8	−9.9
$CH_3CH_2CH(NO_2)CH_3$	1496.9	81.9	1415.1	−40.0	−47.4	−39.1	−8.3
CH_3CH_2–O–CH_2CH_3	1395.4	82.3	1313.1	−57.9	−65.0	−60.3	−4.7
CH_3–$CH(OCH_3)_2$	1488.5	85.6	1403.0	−88.8	−96.3	−93.1	−3.2
$(CH_3)_3$C–SH (*t*-butanethiole)	1363.4	78.7	1284.7	−22.8	−29.8	−26.2	−3.6
$(CH_3CH_2S)_2$	1426.1	81.2	1344.8	−17.3	−24.1	−17.9	−6.2
$(CH_3)_3$C–NH_2 (*t*-butylamine)	1474.5	89.3	1385.2	−24.8	−33.0	−28.9	−4.1
$Si(CH_3)_4$ (tetramethyl silane)	1539.4	88.0	1451.4	−45.3	−52.6	−55.7	3.1
C_5H_6S (2-methyl thiopehene)	1273.3	57.0	1216.3	9.0	5.0	20.0	−15.0
C_5H_7N (*N*-methyl pyrrole)	1377.7	66.5	1311.3	12.6	7.4	24.6	−17.2
$C_5H_{10}O$ (tetrahydropyran)	1567.6	88.3	1479.3	−54.1	−62.3	−53.4	−8.9
$C_2H_5COC_2H_5$ (diethyl ketone)	1573.9	84.9	1489.0	−63.8	−70.6	−61.6	−9.0
$CH_3COOCH(CH_3)_2$	1687.9	88.1	1599.8	−115.6	−122.9	−115.1	−7.8

Table C.1 : HSE/6-311++G(3df,3pd) standard enthalpies of formation at 298K for the G3 set (kcal/mol)

Molecule	ΣD_e [a]	ZPE [b]	ΣD_0 [c]	$\Delta_f H^\circ_{0K}$	$\Delta_f H^\circ_{298K}$	$\Delta_f H^\circ_{298K}$(exp.)[d]	Dev.[e]
$C_5H_{10}S$ (tetrahydrothiopyran)	1535.3	86.1	1449.2	−17.3	−25.2	−15.2	−10.0
$C_5H_{10}NH$ (piperidine)	1638.9	95.8	1543.1	−12.8	−22.0	−11.3	−10.7
$(CH_3)_3C–O–CH_3$	1690.4	98.6	1591.7	−63.3	−71.8	−67.8	−4.0
$C_6H_4F_2$ (1,3-difluorobenzene)	1408.8	50.8	1358.0	−94.7	−97.9	−73.9	−24.0
$C_6H_4F_2$ (1,4-difluorobenzene)	1408.0	50.7	1357.3	−93.9	−97.2	−73.3	−23.9
C_6H_5F (fluorobenzene)	1397.2	55.6	1341.7	−45.2	−48.9	−27.7	−21.2
$(CH_3)_2CH–O–CH(CH_3)_2$	1990.2	115.8	1874.4	−72.7	−82.8	−76.3	−6.5
PF_5	540.8	10.3	530.5	−362.7	−365.2	−381.1	15.9
SF_6	468.6	13.2	455.4	−279.0	−282.2	−291.7	9.5
P_4	293.7	3.9	289.8	11.9	10.1	14.1	−4.0
SO_3	333.7	7.7	326.0	−83.3	−84.7	−94.6	9.9
SCl_2	131.2	1.8	129.4	−6.6	−6.8	−4.2	−2.6
$POCl_3$	357.1	6.0	351.1	−130.9	−132.3	−133.8	1.5
PCl_5	315.6	5.3	310.3	−91.9	−93.1	−86.1	−7.0
SO_2Cl_2	328.1	7.6	320.5	−79.6	−81.1	−84.8	3.7
PCl_3	235.3	3.0	232.3	−71.1	−71.8	−69.0	−2.8
S_2Cl_2	202.7	2.8	199.8	−11.3	−11.7	−4.0	−7.7
$SiCl_2$ ($^1A_1$)	205.8	1.6	204.2	−40.4	−40.3	−40.3	−0.0
CF_3Cl	438.3	9.5	428.8	−174.8	−175.9	−169.5	−6.4

Table C.1 : HSE/6-311++G(3df,3pd) standard enthalpies of formation at 298K for the G3 set (kcal/mol)

Molecule	ΣD_e [a]	ZPE [b]	ΣD_0 [c]	$\Delta_f H^\circ_{0K}$	$\Delta_f H^\circ_{298K}$	$\Delta_f H^\circ_{298K}$(exp.)[d]	Dev.[e]
C_2F_6	797.3	18.5	778.9	−328.1	−330.0	−321.3	−8.7
CF_3	352.1	7.6	344.5	−119.1	−119.7	−111.3	−8.4
C_6H_5 (phenyl radical)	1268.9	51.3	1217.6	60.5	57.5	81.2	−23.7

[a] Electronic atomization energy

[b] Zero point energy correction from scaled HF/6-31G* frequency calculation

[c] Zero point energy corrected atomization energy

[d] Experimental data compiled in Refs. [36, 38]

[e] Theory − Experiment

Table C.2 : HSE/6-311++G(3df,3pd) optimized bond lengths (Å)

Molecule	r_e (exp.)	r_e	Deviation
H_2 ($^1\Sigma_g^+$)	0.741	0.744	0.002
Li_2 ($^1\Sigma_g^+$)	2.673	2.706	0.033
LiH ($^1\Sigma^+$)	1.595	1.592	−0.003
LiF ($^1\Sigma^+$)	1.564	1.569	0.006
LiCl ($^1\Sigma^+$)	2.021	2.017	−0.004
LiO ($^2\Pi$)	1.688	1.688	−0.001
Be_2 ($^1\Sigma_g^+$)	2.440	2.479	0.039
BeH ($^2\Sigma^+$)	1.343	1.345	0.002
BeF ($^2\Sigma^+$)	1.361	1.362	0.001
BeO ($^1\Sigma^+$)	1.331	1.316	−0.015
BeS ($^1\Sigma^+$)	1.742	1.733	−0.008
B_2 ($^3\Sigma_g^-$)	1.590	1.610	0.020
BH ($^1\Sigma^+$)	1.232	1.236	0.004
BF ($^1\Sigma^+$)	1.263	1.258	−0.005
BF_3 (D_{3h})	1.313	1.307	−0.006
BCl ($^1\Sigma^+$)	1.715	1.714	−0.001
BCl_3 (D_{3h})	1.742	1.735	−0.007
BN ($^3\Pi$)	1.281	1.313	0.032
BO ($^2\Sigma^+$)	1.204	1.198	−0.007
BS ($^2\Sigma^+$)	1.609	1.605	−0.004
C_2 ($^1\Sigma_g^+$)	1.242	1.245	0.002
CH ($^2\Pi$)	1.120	1.122	0.002
CH_4 ($^1A_1, T_d$)	1.087	1.087	0.000
CF ($^2\Pi$)	1.272	1.266	−0.006
CF_4 ($^1A_1, T_d$)	1.323	1.316	−0.007
CCl ($^2\Pi$)	1.645	1.642	−0.003
CCl_4 ($^1A_1, T_d$)	1.767	1.762	−0.005

Table C.2 : HSE/6-311++G(3df,3pd) optimized bond lengths (Å)

Molecule	r_e (exp.)	r_e	Deviation
CN ($^2\Sigma^+$)	1.172	1.159	−0.013
CO ($^1\Sigma^+$)	1.128	1.122	−0.006
CO^+ ($^2\Sigma^+$)	1.115	1.105	−0.010
CO_2 ($^1\Sigma_g^+$)	1.160	1.155	−0.005
CP ($^2\Sigma^+$)	1.562	1.548	−0.014
CS ($^1\Sigma^+$)	1.535	1.528	−0.007
CS_2 ($^1\Sigma_g^+$)	1.553	1.548	−0.005
N_2 ($^1\Sigma_g^+$)	1.098	1.089	−0.009
N_2^+ ($^2\Sigma_g^+$)	1.116	1.101	−0.015
NH ($^3\Sigma^-$)	1.036	1.036	0.000
NH^+ ($^2\Pi$)	1.070	1.074	0.004
NF ($^3\Sigma^-$)	1.317	1.302	−0.015
NCl ($^3\Sigma^-$)	1.611	1.601	−0.009
NO ($^2\Pi$)	1.151	1.139	−0.012
NO^+ ($^1\Sigma^+$)	1.063	1.053	−0.010
NS ($^2\Pi$)	1.494	1.483	−0.011
O_2 ($^3\Sigma_g^-$)	1.208	1.191	−0.016
O_2^+ ($^2\Pi_g$)	1.116	1.097	−0.019
OH ($^2\Pi$)	0.970	0.970	0.000
OH^+ ($^3\Sigma^-$)	1.029	1.030	0.002
OF ($^2\Pi$)	1.358	1.328	−0.030
F_2 ($^1\Sigma_g^+$)	1.412	1.375	−0.036
F_2^+ ($^2\Pi_g$)	1.322	1.272	−0.050
HF ($^1\Sigma^+$)	0.917	0.917	0.001
HF^+ ($^2\Pi$)	1.001	1.006	0.004
Na_2 ($^1\Sigma_g^+$)	3.079	3.064	−0.015
NaH ($^1\Sigma^+$)	1.887	1.879	−0.008
NaF ($^1\Sigma^+$)	1.926	1.927	0.001

Table C.2 : HSE/6-311++G(3df,3pd) optimized bond lengths (Å)

Molecule	r_e (exp.)	r_e	Deviation
NaCl ($^1\Sigma^+$)	2.361	2.363	0.002
NaO ($^2\Pi$)	2.052	2.049	−0.002
MgH ($^2\Sigma^+$)	1.730	1.737	0.008
MgF ($^2\Sigma^+$)	1.750	1.762	0.012
MgCl ($^2\Sigma^+$)	2.196	2.208	0.012
MgO ($^1\Sigma^+$)	1.748	1.731	−0.017
Al_2 ($^3\Sigma_g^-$)	2.466	2.470	0.004
AlH ($^1\Sigma^+$)	1.648	1.661	0.013
AlF ($^1\Sigma^+$)	1.654	1.672	0.018
AlCl ($^1\Sigma^+$)	2.130	2.144	0.014
AlO ($^2\Sigma^+$)	1.618	1.619	0.001
AlS ($^2\Sigma^+$)	2.029	2.029	0.000
Si_2 ($^3\Sigma_g^-$)	2.246	2.252	0.006
SiH ($^2\Pi$)	1.520	1.528	0.008
SiH_4 ($^1A_1, T_d$)	1.480	1.481	0.001
SiF ($^2\Pi$)	1.601	1.618	0.017
SiF_4 ($^1A_1, T_d$)	1.553	1.563	0.010
SiCl ($^2\Pi$)	2.058	2.067	0.009
$SiCl_4$ ($^1A_1, T_d$)	2.019	2.020	0.001
SiN ($^2\Sigma^+$)	1.572	1.561	−0.011
SiO ($^1\Sigma^+$)	1.510	1.507	−0.003
SiS ($^1\Sigma^+$)	1.929	1.929	−0.000
P_2 ($^1\Sigma_g^+$)	1.893	1.879	−0.014
P_4 ($^1A_1, T_d$)	2.210	2.182	−0.028
PH ($^3\Sigma^-$)	1.421	1.425	0.003
PF ($^3\Sigma^-$)	1.589	1.600	0.011
PCl ($^3\Sigma^-$)	2.015	2.013	−0.002
PN ($^1\Sigma^+$)	1.491	1.477	−0.014

Table C.2 : HSE/6-311++G(3df,3pd) optimized bond lengths (Å)

Molecule	r_e (exp.)	r_e	Deviation
PO ($^2\Pi$)	1.476	1.471	−0.005
S_2 ($^3\Sigma_g^-$)	1.889	1.885	−0.004
SH ($^2\Pi$)	1.341	1.343	0.003
SF ($^2\Pi$)	1.601	1.600	−0.000
SF_6 ($^1A_{1g}, O_h$)	1.561	1.565	0.004
SO ($^3\Sigma^-$)	1.481	1.478	−0.003
SO_3 ($^1A_1', D_{3h}$)	1.420	1.417	−0.002
Cl_2 ($^1\Sigma_g^+$)	1.988	1.980	−0.008
Cl_2^+ ($^2\Pi_g$)	1.891	1.883	−0.008
HCl ($^1\Sigma^+$)	1.275	1.277	0.002
HCl^+ ($^2\Pi$)	1.315	1.319	0.004
ClF ($^1\Sigma^+$)	1.628	1.623	−0.006
ClO ($^2\Pi$)	1.570	1.559	−0.010

Table C.3 : HSE/6-311++G(3df,3pd) frequencies (cm^{-1})

Molecule	ω_e (exp.)	ω_e	Deviation
H_2 ($^1\Sigma_g^+$)	4401.2	4421.8	20.6
Li_2 ($^1\Sigma_g^+$)	351.4	347.1	−4.4
LiH ($^1\Sigma^+$)	1405.7	1425.5	19.8
LiF ($^1\Sigma^+$)	910.6	913.8	3.2
LiCl ($^1\Sigma^+$)	643.0	645.7	2.7
LiO ($^2\Pi$)	814.6	820.9	6.3
LiNa ($^1\Sigma^+$)	256.8	257.8	1.0
Be_2 ($^1\Sigma_g^+$)	267.9	311.1	43.2
BeH ($^2\Sigma^+$)	2060.8	2060.7	−0.1
BeH^+ ($^1\Sigma^+$)	2221.7	2216.5	−5.2
BeF ($^2\Sigma^+$)	1247.4	1257.2	9.8
BeCl ($^2\Sigma^+$)	846.7	846.4	−0.3
BeO ($^1\Sigma^+$)	1487.3	1573.7	86.4
BeS ($^1\Sigma^+$)	997.9	1028.6	30.6
B_2 ($^3\Sigma_g^-$)	1051.3	1026.0	−25.3
BH ($^1\Sigma^+$)	2366.9	2350.2	−16.7
BF ($^1\Sigma^+$)	1402.1	1416.7	14.6
BCl ($^1\Sigma^+$)	840.3	844.4	4.1
BN ($^3\Pi$)	1514.6	1602.2	87.6
BO ($^2\Sigma^+$)	1885.7	1945.6	59.9
BS ($^2\Sigma^+$)	1180.2	1208.6	28.4
C_2 ($^1\Sigma_g^+$)	1854.7	1902.4	47.7
CH ($^2\Pi$)	2858.5	2873.5	15.0
CF ($^2\Pi$)	1308.1	1333.6	25.5
CN ($^2\Sigma^+$)	2068.6	2186.4	117.8
CO ($^1\Sigma^+$)	2169.8	2244.8	75.0
CO^+ ($^2\Sigma^+$)	2214.2	2342.7	128.5

Table C.3 : HSE/6-311++G(3df,3pd) frequencies (cm^{-1})

Molecule	ω_e (exp.)	ω_e	Deviation
CP ($^2\Sigma^+$)	1239.7	1308.3	68.7
CS ($^1\Sigma^+$)	1285.2	1336.6	51.4
N_2 ($^1\Sigma_g^+$)	2358.6	2482.4	123.8
N_2^+ ($^2\Sigma_g^+$)	2207.0	2372.9	165.9
NH ($^3\Sigma^-$)	3282.3	3332.0	49.7
NF ($^3\Sigma^-$)	1141.4	1206.8	65.4
NCl ($^3\Sigma^-$)	828.0	868.7	40.8
NO ($^2\Pi$)	1904.2	2035.2	131.0
NO^+ ($^1\Sigma^+$)	2376.4	2536.5	160.1
NS ($^2\Pi$)	1218.7	1296.1	77.4
O_2 ($^3\Sigma_g^-$)	1580.2	1720.7	140.5
O_2^+ ($^2\Pi_g$)	1904.8	2141.0	236.2
OH ($^2\Pi$)	3737.8	3776.6	38.8
OH^+ ($^3\Sigma^-$)	3113.4	3111.7	−1.7
F_2 ($^1\Sigma_g^+$)	916.6	1084.7	168.0
F_2^+ ($^2\Pi_g$)	1073.3	1294.2	220.9
HF ($^1\Sigma^+$)	4138.3	4159.7	21.3
HF^+ ($^2\Pi$)	3090.5	3057.6	−32.9
Na_2 ($^1\Sigma_g^+$)	159.1	163.9	4.8
NaH ($^1\Sigma^+$)	1172.2	1178.6	6.4
NaF ($^1\Sigma^+$)	535.7	535.5	−0.2
NaO ($^2\Pi$)	492.3	491.6	−0.7
MgH ($^2\Sigma^+$)	1495.2	1481.4	−13.8
MgH^+ ($^1\Sigma^+$)	1699.1	1732.3	33.2
MgO ($^1\Sigma^+$)	784.8	833.1	48.3
MgS ($^1\Sigma^+$)	528.7	547.5	18.8
Al_2 ($^3\Sigma_g^-$)	350.0	352.0	1.9
AlH ($^1\Sigma^+$)	1682.6	1654.3	−28.3

Table C.3 : HSE/6-311++G(3df,3pd) frequencies (cm^{-1})

Molecule	ω_e (exp.)	ω_e	Deviation
AlF ($^1\Sigma^+$)	802.3	770.6	−31.7
AlCl ($^1\Sigma^+$)	481.3	471.8	−9.5
AlO ($^2\Sigma^+$)	979.2	964.0	−15.3
AlS ($^2\Sigma^+$)	617.1	622.7	5.6
Si_2 ($^3\Sigma_g^-$)	511.0	518.9	7.9
SiH ($^2\Pi$)	2041.8	2029.3	−12.5
SiH^+ ($^1\Sigma^+$)	2157.2	2131.2	−26.0
SiF ($^2\Pi$)	857.2	828.0	−29.1
SiCl ($^2\Pi$)	535.6	530.2	−5.4
SiN ($^2\Sigma^+$)	1151.4	1200.1	48.7
SiO ($^1\Sigma^+$)	1241.5	1271.3	29.7
SiS ($^1\Sigma^+$)	749.6	765.1	15.4
P_2 ($^1\Sigma_g^+$)	780.8	834.6	53.8
P_2^+ ($^2\Pi_u^+$)	672.2	727.4	55.2
PH ($^3\Sigma^-$)	2365.2	2385.8	20.6
PF ($^3\Sigma^-$)	846.8	837.1	−9.6
PCl ($^3\Sigma^-$)	551.4	558.5	7.1
PN ($^1\Sigma^+$)	1337.2	1435.7	98.5
PO ($^2\Pi$)	1233.3	1284.7	51.4
S_2 ($^3\Sigma_g^-$)	725.6	751.9	26.2
SO ($^3\Sigma^-$)	1149.2	1199.0	49.8
Cl_2 ($^1\Sigma_g^+$)	559.7	575.8	16.1
Cl_2^+ ($^2\Pi_g$)	645.6	675.5	29.9
HCl ($^1\Sigma^+$)	2990.9	3008.8	17.9
HCl^+ ($^2\Pi$)	2673.7	2685.5	11.8
ClF ($^1\Sigma^+$)	786.1	818.8	32.7
ClO ($^2\Pi$)	853.8	901.2	47.4

Table C.4 : HSE/6-311++G(3df,3pd) ionization potentials (eV)

Molecule	IP (exp.)	IP	Deviation
Li $(^2S) \rightarrow Li^+ (^1S)$	5.39	5.72	0.33
Be $(^1S) \rightarrow Be^+ (^2S)$	9.32	9.18	−0.14
B $(^2P) \rightarrow B^+ (^1S)$	8.30	8.90	0.60
C $(^3P) \rightarrow C^+ (^2P)$	11.26	11.78	0.52
N $(^4S) \rightarrow N^+ (^3P)$	14.53	14.98	0.44
O $(^3P) \rightarrow O^+ (^4S)$	13.62	14.16	0.55
F $(^2P) \rightarrow F^+ (^3P)$	17.42	17.77	0.35
Na $(^2S) \rightarrow Na^+ (^1S)$	5.14	5.46	0.32
Mg $(^1S) \rightarrow Mg^+ (^2S)$	7.65	7.74	0.09
Al $(^2P) \rightarrow Al^+ (^1S)$	5.99	6.30	0.31
Si $(^3P) \rightarrow Si^+ (^2P)$	8.15	8.44	0.29
P $(^4S) \rightarrow P^+ (^3P)$	10.49	10.76	0.27
S $(^3P) \rightarrow S^+ (^4S)$	10.36	10.66	0.30
Cl $(^2P) \rightarrow Cl^+ (^3P)$	12.97	13.22	0.25
CH_4 $(^1A_1) \rightarrow CH_4^+ (^2B_2)$	12.61	12.66	0.05
NH_3 $(^1A_1) \rightarrow NH_3^+ (^2A_2'')$	10.07	10.29	0.22
OH $(^2\Pi) \rightarrow OH^+ (^3\Sigma^-)$	13.02	13.28	0.26
H_2O $(^1A_1) \rightarrow H_2O^+ (^2B_1)$	12.62	12.71	0.09
HF $(^1\Sigma^+) \rightarrow HF^+ (^2\Pi)$	16.04	16.17	0.13
SiH_4 $(^1A_1) \rightarrow SiH_4^+ (^2A')$	11.00	11.05	0.05
PH $(^3\Sigma^-) \rightarrow PH^+ (^2\Pi)$	10.15	10.52	0.37
PH_2 $(^2B_1) \rightarrow PH_2^+ (^1A_1)$	9.82	10.26	0.43
PH_3 $(^1A_1) \rightarrow PH_3^+ (^2A_1)$	9.87	9.97	0.10
SH $(^2\Pi) \rightarrow SH^+ (^3\Sigma^-)$	10.42	10.60	0.18
H_2S $(^1A_1) \rightarrow H_2S^+ (^2B_1)$	10.46	10.59	0.14
HCl $(^1\Sigma^+) \rightarrow HCl^+ (^2\Pi)$	12.75	12.92	0.17
HC≡CH $(^1\Sigma_g^+) \rightarrow$ HC≡CH$^+$ $(^2\Pi_u)$	11.40	11.39	−0.01

Table C.4 : HSE/6-311++G(3df,3pd) ionization potentials (eV)

Molecule	IP (exp.)	IP	Deviation
CH_2=CH_2 (^1A_g) → CH_2=CH_2^+ ($^2B_{3u}$)	10.51	10.52	0.01
CO ($^1\Sigma^+$) → CO^+ ($^2\Sigma^+$)	14.01	14.18	0.17
N_2 ($^1\Sigma_g^+$) → N_2^+ ($^2\Sigma_g^+$)	15.58	16.02	0.44
O_2 ($^3\Sigma_g^-$) → O_2^+ ($^2\Pi_g$)	12.07	13.03	0.96
P_2 ($^1\Sigma_g^+$) → P_2^+ ($^2\Pi_u$)	10.53	10.58	0.05
S_2 ($^3\Sigma_g^-$) → S_2^+ ($^2\Pi_g$)	9.36	9.89	0.53
Cl_2 ($^1\Sigma_g^+$) → Cl_2^+ ($^2\Pi_g$)	11.48	11.60	0.12
ClF ($^1\Sigma^+$) → ClF^+ ($^2\Pi$)	12.66	12.77	0.11
CS ($^1\Sigma^+$) → CS^+ ($^2\Sigma^+$)	11.33	11.54	0.21
H (^2S) → H^+	13.60	13.91	0.31
He (^1S) → He^+ (^2S)	24.59	24.76	0.17
Ne (^1S) → Ne^+ (^2P)	21.56	21.79	0.23
Ar (^1S) → Ar^+ (^2P)	15.76	15.99	0.23
BF_3 ($^1A_1'$) → BF_3^+ ($^2B_2$)	15.56	15.62	0.06
BCl_3 ($^1A_1'$) → BCl_3^+ ($^2B_2$)	11.60	11.59	−0.01
B_2F_4 ($^1A_1$) → $B_2F_4^+$ ($^2A_1$)	12.07	11.68	−0.39
CO_2 ($^1\Sigma_g^+$) → CO_2^+ ($^2\Pi_g$)	13.77	13.84	0.07
CF_2 ($^1A_1$) → CF_2^+ ($^2A_1$)	11.44	11.39	−0.05
COS ($^1\Sigma^+$) → COS^+ ($^2\Pi$)	11.18	11.41	0.23
CS_2 ($^1\Sigma_g^+$) → CS_2^+ ($^2\Pi_g$)	10.07	10.26	0.19
CH_2 ($^3B_1$) → CH_2^+ ($^2A_1$)	10.40	10.74	0.35
CH_3 ($^2A_2''$) → CH_3^+ ($^1A_1'$)	9.84	10.27	0.43
C_2H_5 ($^2A'$) → $C_2H_5^+$ ($^1A_1$)	8.12	8.43	0.31
C_3H_4 ($^1A_1$) → $C_3H_4^+$ ($^2B_1$) (cyclopropene)	9.67	9.60	−0.07
CH_2=C=CH_2 ($^1A_1$) → CH_2=C=CH_2^+ (^2A)	9.69	9.63	−0.07
$(CH_3)_2CH$ ($^2A'$) → $(CH_3)_2CH^+$ (^1A)	7.37	7.63	0.26
C_6H_6 ($^1A_{1g}$) → $C_6H_6^+$ ($^2B_{2g}$)	9.24	9.28	0.04
$C_6H_5CH_3$ ($^1A'$) → $C_6H_5CH_3^+$ ($^2A''$)	8.83	8.84	0.01

Table C.4 : HSE/6-311++G(3df,3pd) ionization potentials (eV)

Molecule	IP (exp.)	IP	Deviation
CN $(^2\Sigma^+) \rightarrow CN^+ (^1\Sigma^+)$	13.60	15.58	1.99
HC=O $(^2A') \rightarrow$ HC=O$^+$ $(^1\Sigma^+)$	8.14	8.71	0.57
CH_2OH $(^2A) \rightarrow CH_2OH^+$ $(^1A')$	7.55	7.92	0.36
CH_3O $(^2A') \rightarrow CH_3O^+$ $(^3A_1)$	10.73	10.79	0.06
CH_3OH $(^1A') \rightarrow CH_3OH^+$ (^2A)	10.85	10.83	−0.02
CH_3F $(^1A_1) \rightarrow CH_3F^+$ $(^2A')$	12.47	12.53	0.06
CH_2S $(^1A_1) \rightarrow CH_2S^+$ $(^2B_2)$	9.38	9.46	0.08
CH_2SH $(^2A) \rightarrow CH_2SH^+$ $(^1A')$	7.54	7.94	0.40
CH_3SH $(^1A') \rightarrow CH_3SH^+$ $(^2A'')$	9.44	9.52	0.08
CH_3Cl $(^1A_1) \rightarrow CH_3Cl^+$ $(^2A')$	11.22	11.35	0.13
C_2H_5OH $(^1A') \rightarrow C_2H_5OH^+$ (^2A)	10.43	10.32	−0.11
CH_3CHO $(^1A') \rightarrow CH_3CHO^+$ $(^2A')$	10.23	10.26	0.03
CH_3OF $(^1A') \rightarrow CH_3OF^+$ $(^2A'')$	11.34	11.29	−0.05
C_2H_4S $(^1A_1) \rightarrow C_2H_4S^+$ $(^2B_1)$ (thiirane)	9.05	9.14	0.09
$(CN)_2$ $(^1\Sigma_g^+) \rightarrow (CN)_2^+$ $(^2\Pi_g)$	13.37	13.15	−0.22
C_4H_4O $(^1A_1) \rightarrow C_4H_4O^+$ $(^2A_2)$ (furan)	8.88	8.88	−0.00
C_4H_4NH $(^1A_1) \rightarrow C_4H_4NH^+$ $(^2A_2)$ (pyrrole)	8.21	8.24	0.04
C_6H_5OH $(^1A') \rightarrow C_6H_5OH^+$ $(^2A'')$	8.49	8.54	0.05
$C_6H_5NH_2$ $(^1A') \rightarrow C_6H_5NH_2^+$ $(^2B_1)$	7.72	7.73	0.01
B_2H_4 $(^1A_1) \rightarrow B_2H_4^+$ $(^2A_1)$	9.70	9.66	−0.04
NH $(^3\Sigma^-) \rightarrow NH^+$ $(^2\Pi)$	13.49	13.99	0.50
NH_2 $(^2B_1) \rightarrow NH_2^+$ $(^3B_1)$	11.14	11.38	0.24
HN=NH $(^1A_g) \rightarrow$ HN=NH$^+$ (^2A_g)	9.59	9.64	0.05
NH_2NH $(^2A) \rightarrow NH_2NH^+$ $(^1A')$	7.61	8.11	0.50
HOF $(^1A') \rightarrow HOF^+$ $(^2A'')$	12.71	12.69	−0.02
SiH_2 $(^1A_1) \rightarrow SiH_2^+$ $(^2A_1)$	9.15	9.17	0.02
SiH_3 $(^2A_1) \rightarrow SiH_3^+$ $(^1A_1)$	8.13	8.47	0.34
Si_2H_2 $(^1A_1) \rightarrow Si_2H_2^+$ $(^2A_1)$	8.20	8.27	0.07

Table C.4 : HSE/6-311++G(3df,3pd) ionization potentials (eV)

Molecule	IP (exp.)	IP	Deviation
Si_2H_4 (^1A_g) $\rightarrow$ $Si_2H_4^+$ ($^2B_{3u}$)	8.09	8.07	-0.02
Si_2H_5 ($^2A'$) $\rightarrow$ $Si_2H_5^+$ ($^1A'$)	7.60	7.98	0.38
Si_2H_6 ($^1A_{1g}$) $\rightarrow$ $Si_2H_6^+$ ($^2A_{1g}$)	9.74	9.76	0.02

Table C.5 : HSE/6-311++G(3df,3pd) electron affinities (eV)

Molecule	EA (exp.)	EA	Deviation
C $(^3P) \rightarrow C^- (^4S)$	1.26	1.62	0.36
O $(^3P) \rightarrow O^- (^2P)$	1.46	1.58	0.12
F $(^2P) \rightarrow F^- (^1S)$	3.40	3.45	0.05
Si $(^3P) \rightarrow Si^- (^4S)$	1.39	1.62	0.24
P $(^4S) \rightarrow P^- (^3P)$	0.75	0.97	0.22
S $(^3P) \rightarrow S^- (^2P)$	2.08	2.27	0.20
Cl $(^2P) \rightarrow Cl^- (^1S)$	3.61	3.81	0.20
CH $(^2\Pi) \rightarrow CH^- (^3\Sigma^-)$	1.24	1.61	0.37
CH_2 $(^3B_1) \rightarrow CH_2^- (^2B_1)$	0.65	0.76	0.11
CH_3 $(^2A_2'') \rightarrow CH_3^- (^1A_1)$	0.08	0.07	−0.01
NH $(^3\Sigma^-) \rightarrow NH^- (^2\Pi)$	0.37	0.44	0.07
NH_2 $(^2B_1) \rightarrow NH_2^- (^1A_1)$	0.77	0.75	−0.02
OH $(^2\Pi) \rightarrow OH^- (^1\Sigma^+)$	1.83	1.79	−0.04
SiH $(^2\Pi) \rightarrow SiH^- (^3\Sigma^-)$	1.28	1.55	0.27
SiH_2 $(^1A_1) \rightarrow SiH_2^- (^2B_1)$	1.12	1.45	0.32
SiH_3 $(^2A_1) \rightarrow SiH_3^- (^1A_1)$	1.41	1.51	0.11
PH $(^3\Sigma^-) \rightarrow PH^- (^2\Pi)$	1.03	1.16	0.13
PH_2 $(^2B_1) \rightarrow PH_2^- (^1A_1)$	1.27	1.37	0.09
SH $(^2\Pi) \rightarrow SH^- (^1\Sigma^+)$	2.31	2.45	0.13
O_2 $(^3\Sigma_g^-) \rightarrow O_2^- (^2\Pi_g)$	0.45	0.56	0.11
NO $(^2\Pi) \rightarrow NO^- (^3\Sigma^-)$	0.03	0.42	0.39
CN $(^2\Sigma^+) \rightarrow CN^- (^1\Sigma^+)$	3.86	4.10	0.23
PO $(^2\Pi) \rightarrow PO^- (^3\Sigma^-)$	1.09	1.54	0.45
S_2 $(^3\Sigma_g^-) \rightarrow S_2^- (^2\Pi_g)$	1.67	1.81	0.14
Cl_2 $(^1\Sigma_g^+) \rightarrow Cl_2^- (^2\Sigma_u^+)$	2.38	2.86	0.48
Li $(^2S) \rightarrow Li^- (^1S)$	0.62	0.56	−0.05
B $(^2P) \rightarrow B^- (^3P)$	0.28	0.62	0.34

Table C.5 : HSE/6-311++G(3df,3pd) electron affinities (eV)

Molecule	EA (exp.)	EA	Deviation
Na $(^2S) \rightarrow Na^- (^1S)$	0.55	0.59	0.04
Al $(^2P) \rightarrow Al^- (^3P)$	0.44	0.63	0.19
C_2 $(^1\Sigma_g^+) \rightarrow C_2^- (^2\Sigma_g^+)$	3.27	4.58	1.31
C=C=O $(^3\Sigma^-) \rightarrow$ C=C=O$^-$ $(^2\Pi)$	2.29	2.41	0.12
CF_2 $(^1A_1) \rightarrow CF_2^- (^2B_1)$	0.17	0.55	0.39
NCO $(^2\Pi) \rightarrow NCO^- (^1\Sigma^+)$	3.61	3.63	0.03
NO_2 $(^2A_1) \rightarrow NO_2^- (^1A_1)$	2.27	2.28	0.01
O_3 $(^1A_1) \rightarrow O_3^- (^2B_1)$	2.10	3.00	0.90
OF $(^2\Pi) \rightarrow OF^- (^1\Sigma^-)$	2.27	2.26	−0.01
SO_2 $(^1A_1) \rightarrow SO_2^- (^2B_1)$	1.11	1.63	0.52
S_2O $(^1A') \rightarrow S_2O^- (^2A'')$	1.88	2.39	0.51
HC≡C $(^2\Sigma^+) \rightarrow$ HC≡C$^-$ $(^1\Sigma^+)$	2.97	3.12	0.15
CH_2=CH $(^2A') \rightarrow CH_2$=CH$^-$ $(^1A')$	0.67	0.72	0.05
CH_2=C=C $(^1A_1) \rightarrow CH_2$=C=C$^-$ $(^2B_1)$	1.79	2.25	0.45
CH_2=C=CH $(^2A') \rightarrow CH_2$=C=CH$^-$ $(^1A')$	0.89	1.05	0.16
CH_2=CHCH_2 $(^2A_2) \rightarrow CH_2$=CHCH_2^- $(^1A_1)$	0.48	0.60	0.12
HC=O $(^2A') \rightarrow$ HC=O$^-$ $(^1A')$	0.31	0.42	0.11
CHF $(^1A') \rightarrow CHF^- (^2A'')$	0.54	0.95	0.41
CH_3O $(^2A') \rightarrow CH_3O^- (^1A')$	1.57	1.64	0.07
CH_3S $(^2A') \rightarrow CH_3S^- (^1A')$	1.87	1.94	0.07
CH_2S $(^1A_1) \rightarrow CH_2S^- (^2A')$	0.47	0.90	0.44
CH_2CN $(^2B_1) \rightarrow CH_2CN^- (^1A')$	1.54	1.64	0.10
CH_2NC $(^2B_1) \rightarrow CH_2NC^- (^1A')$	1.06	1.16	0.10
HC≡CO $(^2A'') \rightarrow$ HC≡CO$^-$ $(^1A')$	2.35	2.38	0.03
CH_2CHO $(^2A'') \rightarrow CH_2CHO^- (^1A')$	1.82	1.95	0.12
CH_3CO $(^2A') \rightarrow CH_3CO^- (^1A')$	0.42	0.41	−0.01
CH_3CH_2O $(^2A'') \rightarrow CH_3CH_2O^- (^1A')$	1.71	1.74	0.03
CH_3CH_2S $(^2A'') \rightarrow CH_3CH_2S^- (^1A')$	1.95	2.02	0.07

Table C.5 : HSE/6-311++G(3df,3pd) electron affinities (eV)

Molecule	EA (exp.)	EA	Deviation
LiH $(^1\Sigma^+) \rightarrow$ LiH$^-$ $(^2\Sigma^+)$	0.34	0.54	0.20
HNO $(^1A')$ $\rightarrow$ HNO$^-$ $(^2A'')$	0.34	0.83	0.49
HOO $(^2A'')$ $\rightarrow$ HOO$^-$ $(^1A')$	1.08	0.96	-0.11

Bibliography

[1] W. Kohn and L. J. Sham, Phys. Rev. **140**, A1133 (1965).

[2] J. P. Perdew, Phys. Rev. Lett. **55**, 1665 (1985).

[3] A. D. Becke, J. Chem. Phys. **98**, 5648 (1993).

[4] J. Tao, J. P. Perdew, V. N. Staroverov, and G. E. Scuseria, Phys. Rev. Lett. **91**, 146401 (2003).

[5] V. N. Staroverov, G. E. Scuseria, J. Tao, and J. P. Perdew, J. Chem. Phys. **119**, 12129 (2003).

[6] V. N. Staroverov, G. E. Scuseria, J. Tao, and J. P. Perdew, Phys. Rev. B **69**, 075102 (2004).

[7] G. E. Scuseria, J. Phys. Chem. **103**, 4782 (1999).

[8] W. Kohn, Int. J. Quantum Chem **56**, 229 (1995).

[9] J. Heyd, G. E. Scuseria, and M. Ernzerhof, J. Chem. Phys. **118**, 8207 (2003).

[10] D. Pines, *Elementary Excitations in Solids* (Perseus Books, Reading, Massachusetts, 1999).

[11] R. D. Adamson, J. P. Dombroski, and P. M. W. Gill, Chem. Phys. Lett. **254**, 329 (1996).

[12] P. M. W. Gill, R. D. Adamson, and J. A. Pople, Mol. Phys. **88**, 1005 (1996).

[13] A. Savin, in *Recent Developments and Applications of Modern Density Functional Theory* (Elsevier Science B. V., Netherlands, 1996), pp. 327–357.

[14] H. Iikura, T. Tsuneda, T. Yanai, and K. Hirao, J. Chem. Phys. **115**, 3540 (2001).

[15] A. Seidl, A. Görling, P. Vogl, and J. A. Majewski, Phys. Rev. B **53**, 3764 (1996).

[16] M. J. Frisch, G. W. Trucks, H. B. Schlegel, G. E. Scuseria, M. A. Robb, J. R. Cheeseman, J. A. Montgomery, Jr., T. Vreven, K. N. Kudin, J. C. Burant, J. M. Millam, S. S. Iyengar, J. Tomasi, V. Barone, B. Mennucci, M. Cossi, G. Scalmani, N. Rega, G. A. Petersson, H. Nakatsuji, M. Hada, M. Ehara, K. Toyota, R. Fukuda, J. Hasegawa, M. Ishida, T. Nakajima, Y. Honda, O. Kitao,

H. Nakai, M. Klene, X. Li, J. E. Knox, H. P. Hratchian, J. B. Cross, C. Adamo, J. Jaramillo, R. Gomperts, R. E. Stratmann, O. Yazyev, A. J. Austin, R. Cammi, C. Pomelli, J. W. Ochterski, P. Y. Ayala, K. Morokuma, G. A. Voth, P. Salvador, J. J. Dannenberg, V. G. Zakrzewski, S. Dapprich, A. D. Daniels, M. C. Strain, O. Farkas, D. K. Malick, A. D. Rabuck, K. Raghavachari, J. B. Foresman, J. V. Ortiz, Q. Cui, A. G. Baboul, S. Clifford, J. Cioslowski, B. B. Stefanov, G. Liu, A. Liashenko, P. Piskorz, I. Komaromi, R. L. Martin, D. J. Fox, T. Keith, M. A. Al-Laham, C. Y. Peng, A. Nanayakkara, M. Challacombe, P. M. W. Gill, B. Johnson, W. Chen, M. W. Wong, C. Gonzalez, and J. A. Pople, *Gaussian Development Version, Revision B.07* (Gaussian, Inc., Pittsburgh PA, 2003).

[17] J. P. Perdew, M. Ernzerhof, and K. Burke, J. Chem. Phys. **105**, 9982 (1996).

[18] M. Ernzerhof, J. P. Perdew, and K. Burke, Int. J. Quant. Chem. **64**, 285 (1997).

[19] M. Ernzerhof and G. E. Scuseria, J. Chem. Phys. **110**, 5029 (1999).

[20] C. Adamo and V. Barone, J. Chem. Phys. **110**, 6158 (1999).

[21] J. P. Perdew, K. Burke, and M. Ernzerhof, Phys. Rev. Lett. **77**, 3865 (1996).

[22] I. Panas, Chem. Phys. Lett. **245**, 171 (1995).

[23] R. D. Adamson, J. P. Dombroski, and P. M. W. Gill, J. Comp. Chem. **20**, 921 (1999).

[24] P. M. W. Gill and J. A. Pople, Int. J. Quant. Chem. **40**, 753 (1991).

[25] M. Ernzerhof and J. P. Perdew, J. Chem. Phys. **109**, 3313 (1998).

[26] M. Abramowitz and I. A. Stegun, in *Handbook of Mathematical Functions*, edited by M. Abramowitz and I. A. Stegun (Dover Publications, Incorporated, Mineola, N.Y., 1977).

[27] E. H. Lieb and S. Oxford, Int. Journal of Quantum Chem. **19**, 427 (1981).

[28] M. Häser and R. Ahlrichs, J. Comp. Chem. **10**, 104 (1989).

[29] L. Greengard and V. Rokhlin, J. Comput. Phys. **73**, 325 (1987).

[30] R. Kutteh, E. Aprà, and J. Nichols, Chem. Phys. Lett. **238**, 173 (1995).

[31] M. C. Strain, G. E. Scuseria, and M. J. Frisch, Science **271**, 51 (1996).

[32] K. N. Kudin and G. E. Scuseria, Chem. Phys. Lett. **289**, 611 (1998).

[33] M. J. Frisch, personal communications (2003) (unpublished).

[34] K. N. Kudin and G. E. Scuseria, Phys. Rev. B **61**, 16440 (2000).

[35] J. C. Burant, G. E. Scuseria, and M. J. Frisch, J. Chem. Phys. **105**, 8969 (1996).

[36] L. A. Curtiss, K. Raghavachari, P. C. Redfern, and J. A. Pople, J. Chem. Phys. **106**, 1063 (1997).

[37] S. J. Chakravorty, S. R. Gwaltney, E. R. Davidson, F. A. Parpia, and C. Froese Fischer, Phys. Rev. A **47**, 3649 (1993).

[38] L. A. Curtiss, K. Raghavachari, P. C. Redfern, V. Rassolov, and J. A. Pople, J. Chem. Phys. **109**, 7764 (1998).

[39] L. A. Curtiss, P. C. Redfern, K. Raghavachari, and J. A. Pople, J. Chem. Phys **109**, 42 (1998).

[40] J. M. Galbraith and H. F. Schaefer III, J. Chem. Phys. **105**, 862 (1996).

[41] J. C. Rienstra-Kiracofe, G. S. Tschumper, H. F. Schaefer III, S. Nandi, and G. B. Ellison, Chem. Rev. **102**, 231 (2002).

[42] N. Rösch and S. B. Trickey, J. Chem. Phys. **106**, 8940 (1997).

[43] W. Koch and M. C. Holthausen, in *A Chemist's Guide to Density Functional Theory* (WILEY-VCH, Weinheim, 2002), Chap. 8.1.2, pp. 127–130.

[44] K. Doll, N. M. Harrison, and V. R. Saunders, J. Phys.: Condens. Matter **11**, 5007 (1999).

[45] J. E. Jaffe, Z. Lin, and A. C. Hess, Phys. Rev. B **57**, 11834 (1998).

[46] J. C. Boettger, U. Birkenheuer, S. Krüger, N. Rösch, and S. B. Trickey, Phys. Rev. B **52**, 2025 (1995).

[47] J. Jaffe, J. Phys. Chem. Solids **55**, 1357 (1994).

[48] M. Catti, G. Valerio, R. Dovesi, and M. Causà, Phys. Rev. B **49**, 14179 (1994).

[49] K. Doll and N. M. Harrison, Chem. Phys. Lett. **317**, (2000).

[50] A. Kokalj, R. Dovesi, and M. Causà, available at http://www.crystal.unito.it (unpublished).

[51] O. Madelung, *Semiconductors - Basic Data*, 2nd ed. (Springer Verlag, Berlin Heidelberg New York, 1996).

[52] S. Adachi, *Optical Properties of Crystalline and Amorphous Semiconductors: Numerical Data and Graphical Information* (Kluwer Academic Pulishers, Dordrecht, 1999).

[53] F. D. Murnaghan, Proc. Natl. Acad. Sci. U.S.A **30**, 244 (1944).

[54] V. I. Anisimov, J. Zaanen, and O. K. Andersen, Phys. Rev. B **44**, 943 (1991).

[55] T. Bredow and A. R. Gerson, Phys. Rev. B **61**, 5194 (2000).

[56] J. Muscat, A. Wander, and N. M. Harrison, Chem. Phys. Lett. **342**, 397 (2001).

[57] J. P. Foster and F. Weinhold, J. Am. Chem. Soc. **102**, 7211 (1980).